nature communications

Article

https://doi.org/10.1038/s41467-024-51850-4

LOXHD1 is indispensable for maintaining TMC1 auditory mechanosensitive channels at the site of force transmission

Received: 1 March 2024

Accepted: 20 August 2024

Published online: 10 September 2024

Check for updates

Pei Wang[1], Katharine K. Miller[1], Enqi He[1], Siddhant S. Dhawan[1], Christopher L. Cunningham[2] & Nicolas Grillet[1]

Hair cell bundles consist of stereocilia arranged in rows of increasing heights, connected by tip links that transmit sound-induced forces to shorter stereocilia tips. Auditory mechanotransduction channel complexes, composed of proteins TMC1/2, TMIE, CIB2, and LHFPL5, are located at the tips of shorter stereocilia. While most components can interact with the tip link in vitro, their ability to maintain the channel complexes at the tip link in vivo is uncertain. Using mouse models, we show that an additional component, LOXHD1, is essential for keeping TMC1-pore forming subunits at the tip link but is dispensable for TMC2. Using SUB-immunogold-SEM, we showed that TMC1 localizes near the tip link but mislocalizes without LOXHD1. LOXHD1 selectively interacts with TMC1, CIB2, LHFPL5, and tip-link protein PCDH15. Our results demonstrate that TMC1-driven mature auditory channels require LOXHD1 to stay connected to the tip link and remain functional, while TMC2-driven developmental channels do not.

Our senses of hearing and touch rely on mechanotransduction (MET), the conversion of mechanical forces into electrical currents. Molecular solutions to MET are radically different between these senses: touch relies mainly on a single molecule forming a mechanosensitive ion channel, PIEZO2[1,2]. Contrarily, hearing requires the assembly of at least four distinct proteins to form a functional mechanosensitive ion channel complex: TMC1/TMC2, TMIE, CIB2, and LHFPL5[3–19]. To sense sound-induced forces, MET proteins must be transported, positioned, and maintained at precise sites within the hair bundle. The hair bundle is an apical membrane specialization of cochlear hair cells composed of an array of actin-filled protrusions called stereocilia, arranged in rows of increasing heights and displaced by sound-induced forces (Fig. 1a, b)[20,21]. Stereocilia from different rows are interconnected by tip links made up of PCDH15 and CDH23, which convey displacement forces to the extreme tip of smaller stereocilia[22–27]. It is at this site, at the membrane of shorter stereocilia tips, that auditory ion channels localize and are mechanically gated by the tip link[28,29] (Fig. 1c).

The MET channel pore is comprised of TMC1 or TMC2, along with a contribution from TMIE[5,6,13]. In rodents, TMC1 and TMC2 are dynamically expressed in cochlear hair cells during development, with TMC2 first present around birth, followed by a short period in which TMC2 and TMC1 are coexpressed (from postnatal day (P)3) and ending with the maintenance of TMC1 alone in mature cochlear hair cells occurring at P7 for outer hair cells (OHCs) and at P11 for inner hair cells (IHCs)[3,13,18,30]. In contrast to these dynamic expression patterns, TMIE, CIB2, and LHFPL5 are expressed at the earliest stages at which MET currents can be elicited[7,9,11,12,15,31]. Each channel complex protein interacts with multiple other components, and many depend on other components for their proper localization[7,10–15,32–38]. For instance, in *Tmie*^{KO} and *Cib2*^{KO} hair cells, TMC1 and TMC2 do not localize to the hair bundle[10,13,32], a phenotype that also progressively develops in *Lhfpl5*^{KO} hair cells[14].

The existence of a direct, physical connection between the channel complex and the tip link is supported by two lines of results: First, TMC1/2, TMIE, and LHFPL5 can all bind in vitro to PCDH15, which constitutes the lower part of the tip link[12–15,34,36]. Second, from dominant negative experiments in zebrafish stereocilia: endogenous PCDH15 is redistributed broadly after the overexpression of membrane-bound TMC2a-N-terminal fragments in zebrafish[34]. However, in situ confirmation through high-resolution localization of the MET channel complex components at the tip link insertion site, at the stereocilia tips,

[1]Department of Otolaryngology-Head and Neck Surgery, Stanford University, 240 Pasteur Drive, Stanford, CA, USA. [2]Pittsburgh Hearing Research Center, Department of Otolaryngology, University of Pittsburgh, Pittsburgh, PA 15213, USA. e-mail: ngrillet@stanford.edu

https://doi.org/10.1038/s41467-024-51850-4

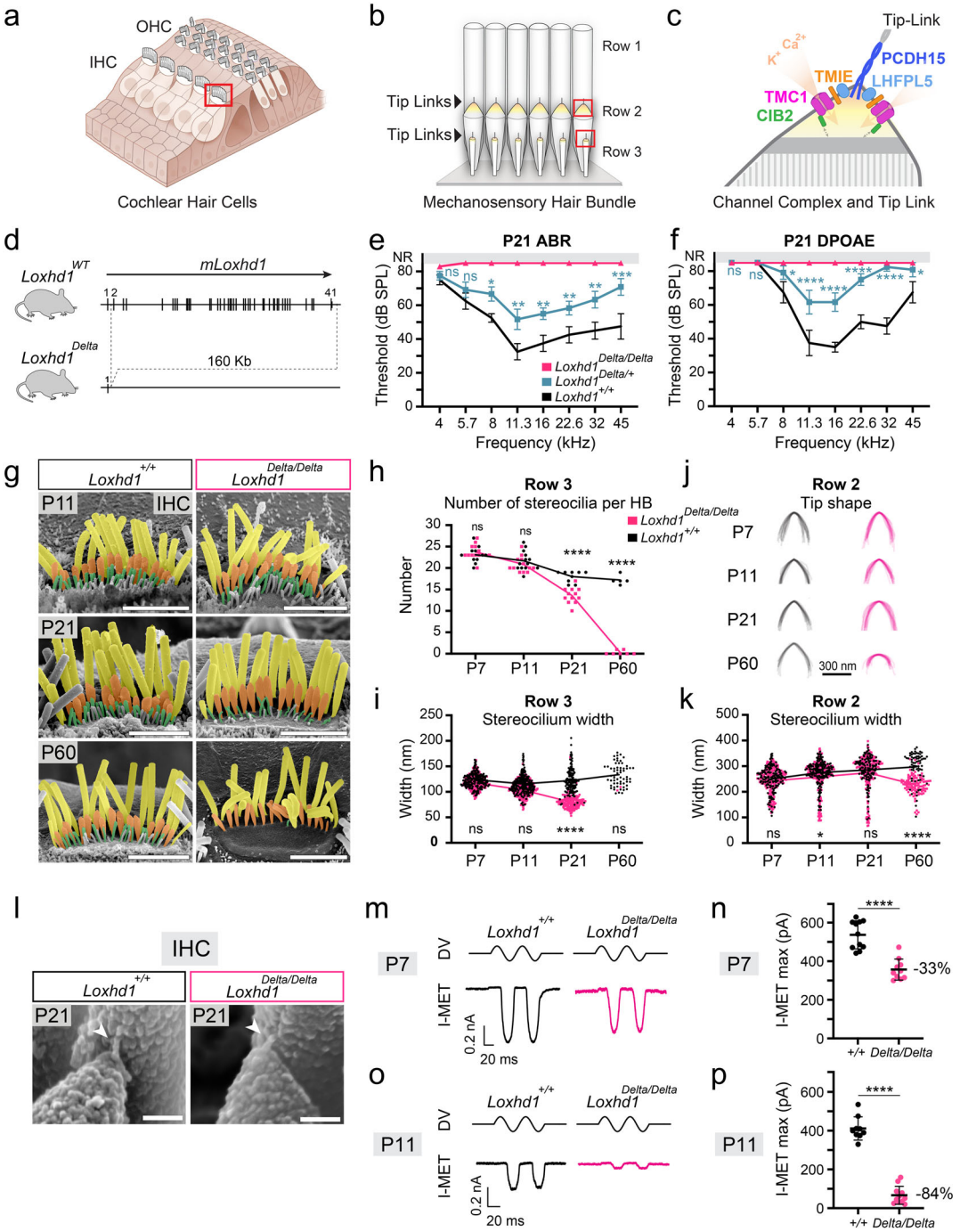

Fig. 1 | The absence of LOXHD1 leads to hair bundle mechanotransduction deficits. a Illustration of a cochlear sensory epithelium, which contains IHCs and OHCs that sense sound-induced forces with their apical hair bundles. **b** Illustration of a P21 IHC hair bundle comprising three stereocilia rows interconnected by tip links. **c** Cartoon representing the known auditory MET channel complex subunits located near the lower tip-link insertion point. **d** The *Loxhd1*^{Delta} allele contains a large-scale genomic deletion at the *Loxhd1* locus (see also Supplementary Fig. 1). **e** ABR and **f** DPOAE thresholds of P21 *Loxhd1*^{Delta} mice across a 4–45 kHz frequency range. Data are represented as mean threshold ± SEM and were obtained from two independent blinded experiments ($n_{animal} \geq 4$). Two-way ANOVA (age/genotype) followed by the Dunnett multiple comparisons test with adjusted *p* values, with wild-type means being the reference. **g** SEM of apical IHC *Loxhd1*^{Delta} mice at P11, P21, and P60, with each stereocilia row being colored in post-production. Similar results were obtained in two independent experiments. Scale bars = 3 μm. **h** Number of row 3 stereocilia in apico-medial *Loxhd1*$^{Delta/Delta}$ IHCs. Means are connected with a line. Per group: P7–P21: $n_{cells} \geq 9$; P60: $n_{cells} \geq 5$; two-way ANOVA followed by the Šídák tests. **i** IHC row 3 stereocilia width. Means are connected with a line. Row 3: Per group: P7–P21: $n_{cells} \geq 9$, $n_{stereocilia} \geq 143$; P60: $n_{cells} \geq 2$, $n_{stereocilia} = 2$ for *Loxhd1*$^{Delta/Delta}$ and $n_{stereocilia} = 61$ for *Loxhd1*$^{Delta/Delta}$. Two-way ANOVA followed by the Šídák tests. **j** IHC row 2 stereocilia tip shape. Superposition of tip traces from 12–20 row 2 stereocilia from 3–4 IHCs from 1–4 animals per genotype. **k** IHC row 2 stereocilia width. Row 2: Per group: P7-P21: $n_{cells} \geq 9$; $n_{stereocilia} \geq 132$; P60: $n_{cells} \geq 5$; $n_{stereocilia} \geq 71$. Micrographs obtained from two independent experiments. Two-way ANOVA followed by the Šídák tests. **l** Tip links (arrowheads) can be detected in P21 *Loxhd1*$^{Delta/Delta}$ apical IHCs. Similar results were obtained in two independent experiments. Scale bars = 100 nm. Mechanotransduction current (I-MET) traces from P7 (**m**) and P11 (**o**) IHC *Loxhd1*$^{+/+}$ and *Loxhd1*$^{Delta/Delta}$ mechanically stimulated with a fluid jet and the maximum I-MET ± SD currents recorded (**n**, **p**). P7: $n_{cells} \geq 10$; P11: $n_{cells} \geq 9$ recorded over more than 12 independent experiments. Unpaired two-tailed *t* test: $^{****}p < 0.0001$. DV = driving voltage of the fluid jet piezoelectric stimulator. HB: hair bundle. For all experiments. ns (non significative) = $p > 0.05$; $^{*}p \leq 0.05$; $^{**}p \leq 0.01$; $^{***}p \leq 0.001$; $^{****}p \leq 0.0001$. The exact *p* values are presented in Supplementary Table 1. Source data are provided as a Source Data file.

is still lacking[30,35,39]. Finally, while the biochemical data involving multiple interactions suggest a strong connection between the channel complex and the tip link, it is unknown whether their combination is sufficient to maintain connectivity in vivo.

Here, we demonstrate that LOXHD1 is an additional MET complex component, critical to preserve the cohesiveness of the complex and the localization of the TMC1 MET channel subunit at the tip link insertion site.

Results

A large-scale genomic deletion of *Loxhd1* in mice leads to semi-dominant hearing loss

Mutations in the gene *LOXHD1* cause recessive hearing loss in humans (DFNB77), mice, and dogs[40–44], but its molecular function remains elusive. LOXHD1 is composed of up to 15 PLAT (polycystin lipoxygenase alpha-toxin) repeats and one coiled-coil domain[40]. To comprehensively characterize the function of the deafness gene *Loxhd1* in hair cells and prevent functional compensation from alternative splicing isoforms, we used CRISPR/Cas9 genomic editing in mouse zygotes to delete 160 kb of the *Loxhd1* locus downstream of the first exon and inactivate all 40 exons encoding the 15 PLAT repeats (Fig. 1d and Supplementary Fig. 1). The deleted interval did not contain other protein-coding genes. We named this allele $Loxhd1^{Delta}$. The $Loxhd1^{Delta/Delta}$ mice were viable and showed no sign of abnormal behavior until at least P30. Additionally, we evaluated the hearing of $Loxhd1^{Delta}$ littermates at P21. The $Loxhd1^{Delta/Delta}$ animals were profoundly deaf, showing no auditory brain stem responses (ABR) at an 80-dB sound pressure level (SPL) across frequencies except for some residual responses at 4 kHz (Fig. 1e)($Loxhd1^{Delta/Delta}$ $n_{animal} = 5$). The hearing of the heterozygous $Loxhd1^{Delta/+}$ animals was also affected, which had ABR thresholds elevated at all frequencies from 8 to 45 kHz compared to wild-type littermates (Dunnett's multiple comparisons test: $Loxhd1^{Delta/+}$ $n = 6$, $Loxhd1^{+/+}$ $n = 4$: $p_{4kHz} = 0.8548$; $p_{5.7kHz} = 0.3666$; $^{*}p_{8kHz} = 0.0215$; $^{**}p_{11.3kHz} = 0.0015$; $^{**}p_{16kHz} = 0.0038$; $^{**}p_{22.6kHz} = 0.0094$; $^{**}p_{32kHz} = 0.0024$; *** $p_{45kHz} = 0.0001$). To test for an OHC dysfunction, we measured the distortion products of otoacoustic emission (DPOAE) of the P21 $Loxhd1^{Delta}$ animals. DPOAE thresholds were not detected at an 80-dB SPL across frequencies in $Loxhd1^{Delta/Delta}$ and were elevated at all frequencies starting at 8 kHz in $Loxhd1^{Delta/+}$ compared with their wild-type littermates (Fig. 1f) ($Loxhd1^{Delta/Delta}$ $n_{animal} = 5$; Dunnett's multiple comparisons test: $Loxhd1^{Delta/+}$ $n = 6$, $Loxhd1^{+/+}$ $n = 4$: p_{4kHz} and $p_{5.7kHz} > 0.9999$; $^{*}p_{8kHz} = 0.0462$; $^{****}p_{11.3kHz} < 0.0001$; $^{****}p_{16kHz} < 0.0001$; $^{****}p_{22.6kHz} < 0.0001$; $^{****}p_{32kHz} < 0.0001$; $^{*}p_{45kHz} = 0.0204$). Therefore, LOXHD1 protein is required for cochlear hair cell function, and appropriate levels are important for optimal function because even partial decreases (i.e., in $Loxhd1^{Delta/+}$) have significant impacts. Thus, the LOXHD1 dosage is crucial for hair cell function and hearing.

Although ABRs were not detected at P21, IHCs and OHCs presented with only mild hair bundle morphological defects: hair bundles of $Loxhd1^{Delta/Delta}$ apical IHCs showed a late thinning and progressive disappearance of row 3 stereocilia at P21 while row 2 tip shape and width were severely affected only at P60 (Fig. 1g–k and Supplementary Fig. 2a–c). Notably, tip links were still detected in P21 $Loxhd1^{Delta/Delta}$ IHC hair bundles (Fig. 1l). Hair bundles of $Loxhd1^{Delta/Delta}$ apical OHCs showed increased variability in the height of row 3 stereocilia at P11 (Supplementary Fig. 2d–f, Supplementary Table 1). Overall, hair cell dysfunction caused by the absence of LOXHD1 appears not to result directly from hair bundle morphological defects but more likely stems from MET defects.

The absence of LOXHD1 induces a progressive IHC MET current reduction at P7 and P11

We previously showed that when LOXHD1 was mutated at the PLAT10 repeat, the MET current amplitudes of homozygous mutant IHCs at P7 were comparable with controls[45]. However, at P11, the amplitudes were subsequently reduced by 95%[45]. In the $Loxhd1^{Delta/Delta}$ animals at the same ages, we measured MET currents using whole-cell patch-clamp generated by fluid jet mechanical stimulation. The deflection of P7 IHC hair bundles toward the tallest stereocilia row of $Loxhd1^{+/+}$ and $Loxhd1^{Delta/Delta}$ produced inward currents (Fig. 1m). However, while the maximum MET current (I-MET) was 537 ± 73 pA (SD) in $Loxhd1^{+/+}$, it was significantly reduced to 357 ± 54 pA in $Loxhd1^{Delta/Delta}$ (Fig. 1n)($Loxhd1^{+/+}$ $n_{cells} = 11$; $Loxhd1^{Delta/Delta}$ $n_{cells} = 10$; Unpaired two-tailed t test: $p < 0.0001$). At P11, the IHC I-MET currents were even further reduced from 412 pA ± 60 pA in $Loxhd1^{+/+}$ to 66 pA ± 46 pA in $Loxhd1^{Delta/Delta}$ littermates (Fig. 1o, p)($Loxhd1^{+/+}n_{cells} = 9$; $Loxhd1^{Delta/Delta}$ $n_{cells} = 11$; Unpaired two-tailed t test: $p < 0.0001$). Therefore, in contrast to our previous work with localized mutations of *Loxhd1*, the complete absence of LOXHD1 leads to earlier effects on IHC MET currents at P7 (33% amplitude reduction), which continues to an 84% reduction at P11. In conclusion, the analysis of the $Loxhd1^{Delta}$ allele has demonstrated that LOXHD1 is required for IHC MET at earlier stages (P7), while it was not required at this time point in the previous PLAT10 *Loxhd1* mutants[45]. Thus, we conclude that functional compensation by *Loxhd1* splicing isoforms occurred in mouse mutations in which LOXHD1 is mutated only in PLAT10. Furthermore, as small MET-currents (-<100 pA) were still detected at P11 in $Loxhd1^{Delta/Delta}$, it appears that some MET channels can still function to a limited degree in mature IHCs when LOXHD1 is absent.

LOXHD1 localizes to the hair bundle and is enriched at the tips of transducing stereocilia

To understand the molecular mechanism by which LOXHD1 affects MET channel function, we determined its localization. We generated a tagged knock-in (KI) mouse, with the insertion of an HA-sequence in the first *Loxhd1* exon before the first PLAT repeat (Fig. 2a and Methods). Homozygous animals for the $Loxhd1^{HA}$ allele showed normal ABR and DPOAE responses at P30, demonstrating that the epitope tag insertion did not affect LOXHD1 and hair cell function (Supplementary Fig. 3a, b). We determined the LOXHD1 expression pattern in cochlear hair bundles from P7 to P21 by immunofluorescence staining against the HA-tag and fluorescent-phalloidin to label stereocilia, comparing the results from $Loxhd1^{HA/HA}$ and non-HA animals. The specific LOXHD1-HA signal was present in P7 hair bundles of both IHCs and OHCs where it appeared to delineate two stereocilia heights, likely corresponding to the tips of row 2 and 3 stereocilia (Fig. 2b). In P11 and P21 IHC hair bundles, which have tall stereocilia rows allowing fine localization, the LOXHD1-HA signal was enriched at the tip of row 2 stereocilia and potentially also at the tip of row 3 stereocilia, which were only weakly stained by phalloidin (Fig. 2c). The LOXHD1-HA staining was also found to a lesser degree along the height of row 1 stereocilia but not with the expected pattern of the upper tip-link insertion sites. The LOXHD1 staining was specific, as it was absent in the non-HA-containing control hair bundles.

To gain a more precise understanding of the distribution of LOXHD1 at the stereocilia tips, we used electron microscopy (EM). Instead of using immunogold-transmission EM (TEM) or immunogold focused-ion beam scanning EM (FIB-SEM), which are cumbersome and restricted to only a small sample number, we improved the existing immunogold-SEM protocols, previously limited to external epitopes[46–49]. We optimized the permeabilization, membrane preservation, antibody penetration, and post-fixation steps. The immunogold signal could then resist the harsh steps of SEM sample preparation. With this method, named SUB-immunogold-SEM and described in an accompanying paper (Miller et al.)[50], we can now detect submembranous epitopes using a secondary antibody conjugated to a gold bead, which will generate backscattered electrons at the cell surface when imaged by SEM. We performed anti-HA SUB-immunogold-SEM on P21 $Loxhd1^{HA/HA}$ IHCs using a 10-nm gold bead

https://doi.org/10.1038/s41467-024-51850-4

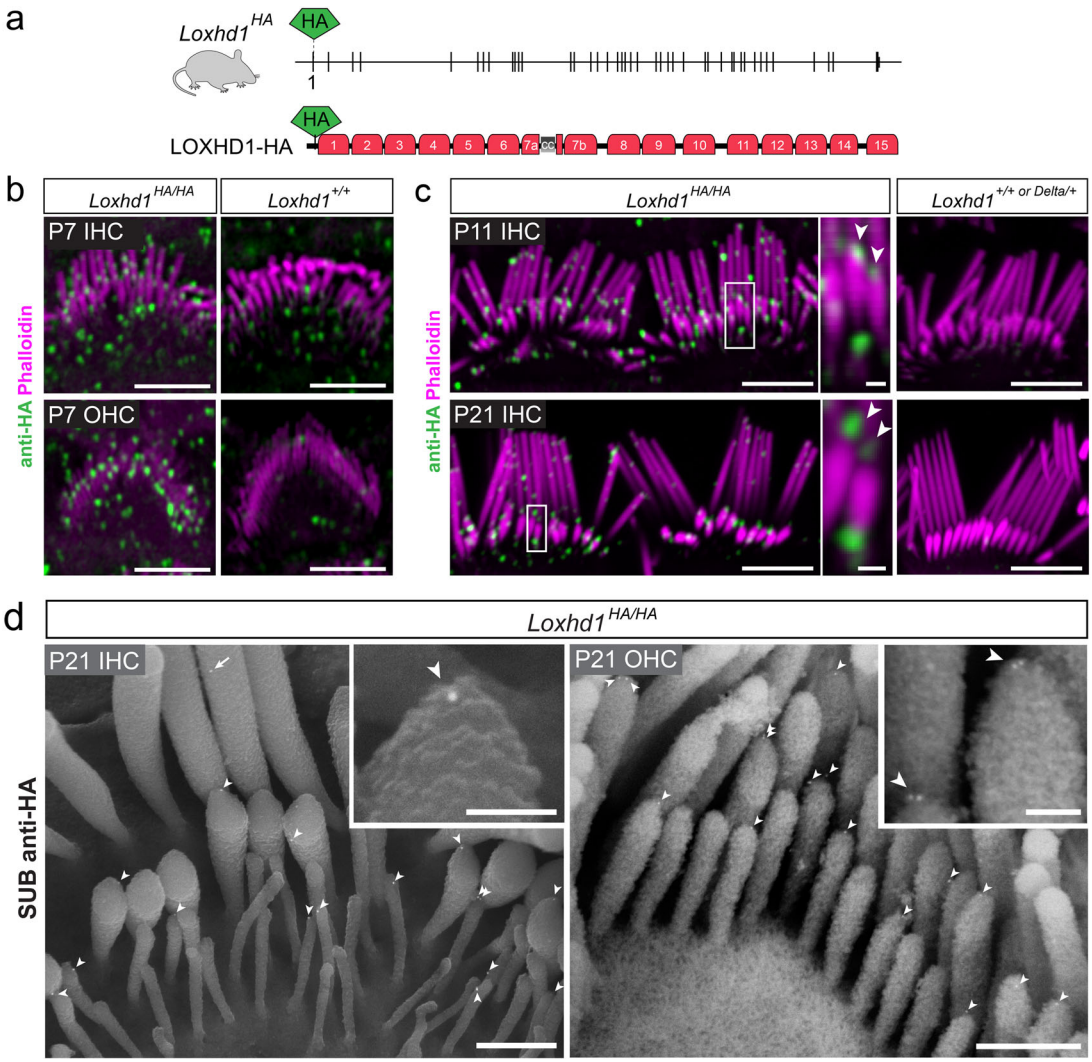

Fig. 2 | LOXHD1 localizes at tips of transducing stereocilia of IHCs and OHCs. **a** The *Loxhd1*^{HA} allele comprises an HA-tag insertion in exon 1 before the first PLAT repeat. **b**, **c** Phalloidin labeling of the actin-rich stereocilia and anti-HA to detect LOXHD1 in *Loxhd1*$^{HA/HA}$ animals by Airyscan super-resolution microscopy. Specific HA staining is detected in *Loxhd1*$^{HA/HA}$ apical IHC and OHC hair bundles at P7 (**b**), P11, and P21 (**c**) but not in negative controls without HA. Scale bars = 4 μm. LOXHD1-HA can clearly be detected at the tip of row 2 stereocilia (arrowheads in insets) of apical P11 and P21 IHCs. Pictures from one of three replicate experiments. Scale bars = 4 μm, Inset scale bars = 0.4 μm. **d** SUB-immunogold-SEM anti-HA detects LOXHD1-associated gold beads on P21 IHC and OHC hair bundles. LOXHD1-gold beads (10 nm) were found at the tips of row 2 and 3 stereocilia (arrowhead) and more rarely in row 1 (arrow). High-magnification insets were taken from different hair bundles. Images from one of two replicate experiments, both yielding similar results. Scale bars = 500 nm, insets 100 nm. Source data are provided as a Source Data file.

conjugated secondary antibody. We detected anti-LOXHD1 gold beads (hereafter referred to as "targeted protein"-gold beads) at the tip of row 2 and row 3 stereocilia of P21 IHCs and OHCs, while none were detected in non-HA animals (Fig. 2d and Supplementary Fig. 3c). We infer from these results that LOXHD1 proteins localized preferentially at the tips of rows 2 and 3, in the same subcellular domain as the MET channel complexes and where the lower part of the tip link inserts into the stereocilia membrane.

The absence of LOXHD1 progressively reduces the number of IHC row 2 stereocilia with TMC1 at their tips

Because the absence of LOXHD1 affected IHC MET current progressively between P7 and P11 while hair bundle morphology remained normal, we hypothesized that one or more components of the mature MET channel complex were selectively affected. The only known channel complex component required for mature hair bundle MET but not for MET during development is TMC1[16]. IHCs first express the paralogue TMC2 from P1–P2, which can compensate for TMC1 deficiency until P7–P10 when TMC2 expression fades away[3,18,30,51]. To test if the lack of LOXHD1 protein would affect TMC1 hair bundle localization, we tracked TMC1 endogenous protein using the *Tmc1*$^{HA/HA}$ KI mice, which we bred with the *Loxhd1*^{Delta} mice[13]. We performed anti-HA immunofluorescence staining on apical IHCs and imaged hair bundles with high-resolution Airyscan microscopy to detect TMC1 at P7, P11, and P21 in littermates and used non-HA animals as negative controls. In the control animals (*Tmc1*$^{HA/HA}$; *Loxhd1*$^{+/+}$), TMC1-HA was detected at low levels in the hair bundle and formed puncta mainly at the tip of row 2 stereocilia at all ages tested (Fig. 3a). In hair cells lacking LOXHD1 (*Tmc1*$^{HA/HA}$; *Loxhd1*$^{Delta/Delta}$) at P7, TMC1-HA was present in the hair bundle and appeared also as puncta at the tip of row 2 stereocilia. However, the number of puncta was reduced compared with the controls (*Tmc1*$^{HA/HA}$; *Loxhd1*$^{+/+}$). To quantify the number of row 2 stereocilia with a punctum at their tip, we used a 3D-surface rendering of the actin-core (labeled with phalloidin) and of the TMC1-HA staining (Supplementary Fig. 4a, Supplementary Movie, and Methods). We then determined the proportion of row 2 stereocilia tips with a

https://doi.org/10.1038/s41467-024-51850-4

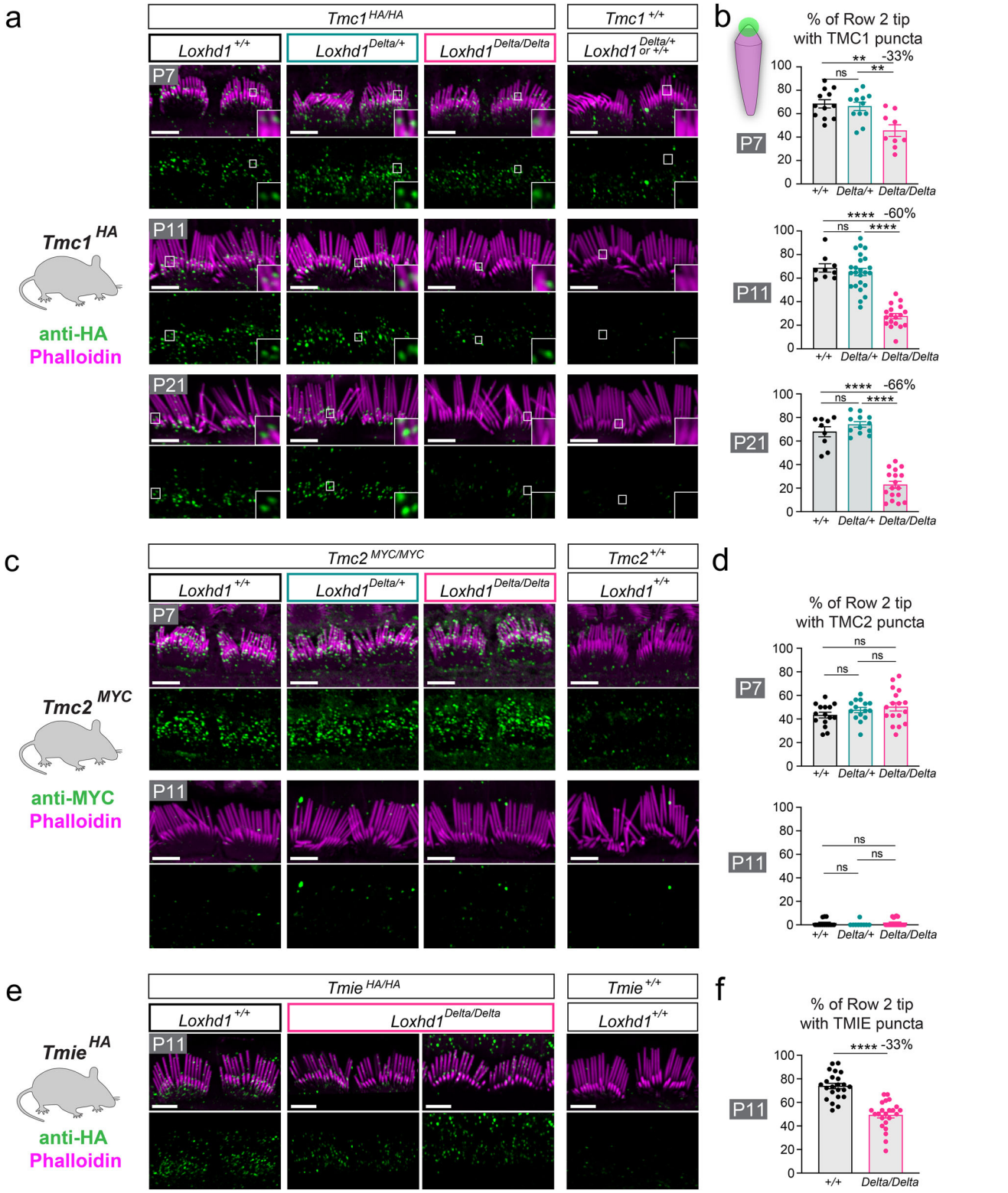

Fig. 3 | TMC1 is progressively missing from row 2 stereocilia tips of IHCs in the absence of LOXHD1. a TMC1 immunofluorescence localization (anti-HA on *Tmc1*$^{HA/HA}$ animals) at the tips of row 2 IHC stereocilia at P7, P11, and P21 showed a progressive reduction in *Loxhd1*$^{Delta/Delta}$ but not in *Loxhd1*$^{Delta/+}$. Insets show high magnification at some row 2 tips. The last panels are negative control animals without a tag. Scale bars = 4 μm. **b** Percentage of row 2 tips with TMC1 puncta identified from 3D-volumes per genotype, represented as mean % ± SEM. (see Supplementary Fig. 2 and the Material and Methods section for more details). Per group: $n_{mice} \geq 3$, $n_{cells} \geq 9$. The experiment was replicated twice at P7 and three times at P11 and P21. One-way ANOVA followed by the Tukey multiple comparisons test. **c** TMC2 immunofluorescence localization (anti-MYC on *Tmc2*$^{MYC/MYC}$ animals) at the tips of row 2 IHC stereocilia at P7 and P11. Scale bars = 4 μm. **d** The percentage of row 2 tips with TMC2 puncta was not affected in *Loxhd1*$^{Delta/Delta}$ at P7 and P11. Represented as mean % ± SEM. The experiment was replicated twice at each age. One-way ANOVA followed by the Tukey multiple comparisons. **e** TMIE immunofluorescence localization (anti-HA on *Tmie*$^{HA/HA}$ animals) at the tips of row 2 IHC stereocilia at P11. Scale bars = 4 μm. **f** The percentage of row 2 tips with TMIE puncta was reduced in *Loxhd1*$^{Delta/Delta}$ at P11 but to a lesser extent than TMC1. Represented as mean % ± SEM. Per group: $n_{mice} = 4$, $n_{cells} = 9$. Unpaired two-tailed *t* test. The experiment was replicated twice. For all experiments. ns (non significative) = $p > 0.05$; *$p \leq 0.05$; **$p \leq 0.01$; ***$p \leq 0.001$; ****$p \leq 0.0001$. The exact *p* values are presented in Supplementary Table 1. Source data are provided as a Source Data file.

punctum per hair bundle. In control hair cells from the P7 *Loxhd1*$^{+/+}$ mice, 68% ± 12% (SEM) of stereocilia per hair bundle had a TMC1 punctum. A similar proportion was found for *Loxhd1*$^{Delta/+}$, while for *Loxhd1*$^{Delta/Delta}$, the proportion of row 2 tips with a TMC1 punctum was significantly reduced to 46% ± 15% (Fig. 3b) (P7: $n_{cells} \geq 9$ per group, One-way ANOVA F (2, 30): $^{***}p = 0.0008$, followed by the Tukey multiple comparisons test: *Loxhd1*$^{Delta/+}$ vs. $^{+/+}$ $p = 0.9156$; *Loxhd1*$^{Delta/Delta}$ vs. $^{+/+}$ $^{**}p = 0.0012$; *Loxhd1*$^{Delta/Delta}$ vs. $^{Delta/+}$ $^{**}p = 0.0031$). As hair cells matured, the proportion of row 2 stereocilia tips with a TMC1 punctum per hair bundle was further reduced to 28 ± 10% at P11 and 23 ± 12% at P21 in *Loxhd1*$^{Delta/Delta}$ (Fig. 3a, b) (P11 and P21: $n_{cells} \geq 9$ per group, One-way ANOVA P11 F (2, 48): $^{****}p < 0.0001$ and P21 F (2, 35): $^{****}p < 0.0001$, followed by the Tukey multiple comparisons test; *Loxhd1*$^{Delta/+}$ vs. $^{+/+}$ P11: $p = 0.7631$, P21: $p = 0.4366$; *Loxhd1*$^{Delta/Delta}$ vs. $^{+/+}$ and *Loxhd1*$^{Delta/Delta}$ vs. $^{Delta/+}$ $^{****}p < 0.0001$ at P11 and P21). Normalized to the wild-type control values at each age, the proportion of TMC1-positive row 2 stereocilia tips decreased by 33% at P7, by 60% at P11, and by 66% at P21 in *Loxhd1*$^{Delta/Delta}$. These results indicate that in IHCs, the absence of LOXHD1 leads to a progressive reduction of the proportion of row 2 stereocilia with TMC1 puncta, a molecular phenotype that is consistent with the progressive reduction in MET current amplitudes. Importantly, IHCs from heterozygous *Loxhd1*$^{Delta/+}$ were not affected by this phenotype.

The absence of LOXHD1 does not affect TMC2 or LHFPL5 localization in the hair bundle but partially affects TMIE

To determine if the absence of LOXHD1 would affect the additional components of the MET channel complex, we localized other known components to the tips of stereocilia in hair bundles using tagged-KI mice or validated antibodies. First, we inspected TMC2 expression using the *Tmc2*^{MYC} allele[13]. At P7, TMC2 was found in the hair bundle and at the tips of row 2 apical IHC stereocilia in the controls (*Tmc2*$^{MYC/MYC}$; *Loxhd1*$^{+/+}$) and had virtually disappeared by P11 (Fig. 3c). The proportion of row 2 stereocilia with TMC2 tip puncta was similar between the *Loxhd1*$^{+/+}$ *and Loxhd1*$^{Delta/Delta}$ animals at P7 (43% ± 9% and 49% ±9%; $n_{cells} \geq 14$ per group, One-way ANOVA F (2, 44): $p = 0.2265$) and at P11 when TMC2 expression faded away (1.5% ± 3% and 1.8% ± 3%; $n_{cells} \geq 9$ per group, One-way ANOVA F (2, 40): $p = 0.6842$) (Fig. 3d). Therefore, the absence of LOXHD1 had no effect on TMC2 hair bundle row 2 tip localization or expression time.

Subsequently, we evaluated TMIE, a component contributing to the channel pore, which is required for localization of TMC1 and TMC2 to the hair bundle[13,32]. To localize TMIE, we used the *Tmie*^{HA} KI allele[13]. At P11, in the apical IHCs of the *Tmie*$^{HA/HA}$; *Loxhd1*$^{+/+}$ control mice, TMIE was found in 74% ± 11% of row 2 tips, while it was reduced to 49% ± 12% in apical IHCs of the *Tmie*$^{HA/HA}$; *Loxhd1*$^{Delta/Delta}$ mice (Fig. 3e, f) ($n_{cells} = 23$ per group, Unpaired two-tailed *t* test: $^{****}p < 0.0001$). Therefore, the absence of LOXHD1 reduces the proportion of row 2 tips with TMIE puncta by 33% at P11.

We then looked at the protein CIB2, an auxiliary component required for TMC1 and TMC2 localization to the hair bundle[10]. We used a commercially available antibody validated on *Cib2*^{KO} hair bundles[7,11]. As in these reports, we obtained a signal along the length of the stereocilia and a weak signal at the tip of row 2 stereocilia in IHCs from the P11 *Loxhd1*$^{+/+}$ mice (Supplementary Fig. 4b). As this signal was still present in the *Loxhd1*$^{Delta/Delta}$ littermates, it appears that the absence of LOXHD1 does not change CIB2 hair bundle localization.

Finally, we examined LHFPL5, whose loss-of-function impacts both the number of tip links and the presence of TMC1 within the hair bundle[14,15]. LHFPL5 was localized with an antibody previously validated on *Lhfpl5*^{KO} cochlear tissue[39]. LHFPL5 was found at the tips of row 2 stereocilia in a similar proportion between *Loxhd1*$^{+/+}$ (81% ±11%) and *Loxhd1*$^{Delta/Delta}$ (78% ±10%) in P11 apical IHCs (Supplementary Fig. 4c, d) ($n_{cells} = 31$ per group, Unpaired two-tailed *t* test: $p = 0.1885$). These results confirm that LHFPL5 localization was not affected by LOXHD1's absence.

Overall, the absence of LOXHD1 had a selective effect on TMC1 row 2 tip localization as three other known MET machinery components—TMC2, CIB2, and LHFPL5—appeared unaffected and as TMIE was only partially affected.

TMC1 normally localizes within 100 nm from the stereocilia tips, where the tip links insert

In addition to the reduction in the number of TMC1 puncta at the tips of row 2 stereocilia found in LOXHD1's absence, we noticed by immunofluorescence that some remaining TMC1 puncta were frequently detected below the row 2 tip at P21 (Supplementary Fig. 5b). However, fluorescence microscopy was unable to distinguish whether this TMC1 signal indicated a mislocalization within row 2 stereocilia or whether it was located at the tips of row 3 stereocilia, which is only weakly stained by phalloidin. To achieve a nanoscale mapping of the TMC1 channel pore-subunits at the stereocilia tips, we used SUB-immunogold-SEM, which allows quantification from large sample numbers[50].

We first determined the TMC1 distribution in mature wild-type IHC hair bundles. We performed anti-HA SUB-immunogold-SEM on control P21 IHCs (*Tmc1*$^{HA/HA}$; *Loxhd1*$^{+/+}$) using a 10-nm gold bead conjugated secondary antibody. We detected TMC1-gold beads at the tips of row 2 and row 3 stereocilia at P21, while none were detected in non-HA animals (Fig. 4a and Supplementary Fig. 5a). We measured the distance from the tips of the stereocilia to the center of the gold beads. The TMC1-gold beads were concentrated within 100 nm from the stereocilia tips in row 2 (81% of all gold beads) and row 3 (100%) (Fig. 4b). Within the first 100 nm, the TMC1-gold beads were further enriched within 50 nm from the tips of row 2 (73%) and row 3 stereocilia (90%) (Fig. 4b, right). Taken together, we demonstrated that in the IHCs of juvenile mice, the TMC1 pore-forming subunits of the auditory MET channels were clustered at the pointiest part of stereocilia tips, where the lower part of the tip link inserts. Further, despite their differences in shape and width of their tips, we found that rows 2 and 3 of P21 IHC stereocilia present similar TMC1 distributions.

TMC1 is progressively mislocalized from the stereocilia tips of IHCs in the absence of LOXHD1

To evaluate at nanoscale the consequences of LOXHD1's absence on TMC1 hair bundle localization, we repeated anti-HA SUB-immunogold-SEM experiments on IHCs from *Loxhd1*$^{+/+}$ and *Loxhd1*$^{Delta/Delta}$ littermates at P7, P11, and P21 (Fig. 4c–e). We measured the distance from the tip of row 2 stereocilia to the center of the gold beads. In control hair cells (*Loxhd1*$^{+/+}$), the TMC1-gold beads were concentrated in the first 100 nm of the row 2 tips with age (69% at P7, 85% at P11, and 81% at P21). In *Loxhd1*$^{Delta/Delta}$ hair cells, the TMC1-gold beads were far less concentrated in the first 100 nm from row 2 tips (38% at P7, 44% at P11, and 8% at P21) and were progressively found at a longer distance from the stereocilia tips, culminating at P21 when the beads were distributed broadly all along the length of the stereocilia (Fig. 4f). We also measured the distance from the tip of row 3 stereocilia to the TMC1-gold beads at P11 and P21 in wild-type IHCs, and found an even stronger concentration in the first 100 nm (99% at P11 and 100% at P21) (Fig. 4g). On a *Loxhd1*$^{Delta/Delta}$ background, the TMC1-gold beads were hardly found in row 3 stereocilia, and the few found at P11 were mainly within the first 100 nm.

To determine how this altered TMC1 distribution affected the number of activatable stereocilia (defined as stereocilia with TMC1 next to the pointiest part of the stereocilia tip, where the tip link inserts), we performed a second analysis: we classified stereocilia according to the presence or absence of the TMC1-gold beads either at any distance from the tip or within the first 100 nm. The number of row 2 stereocilia with gold at any position decreased in the absence of LOXHD1 by 38% at P7, by 31% at P11, and by 57% at P21 (Fig. 4h)

https://doi.org/10.1038/s41467-024-51850-4

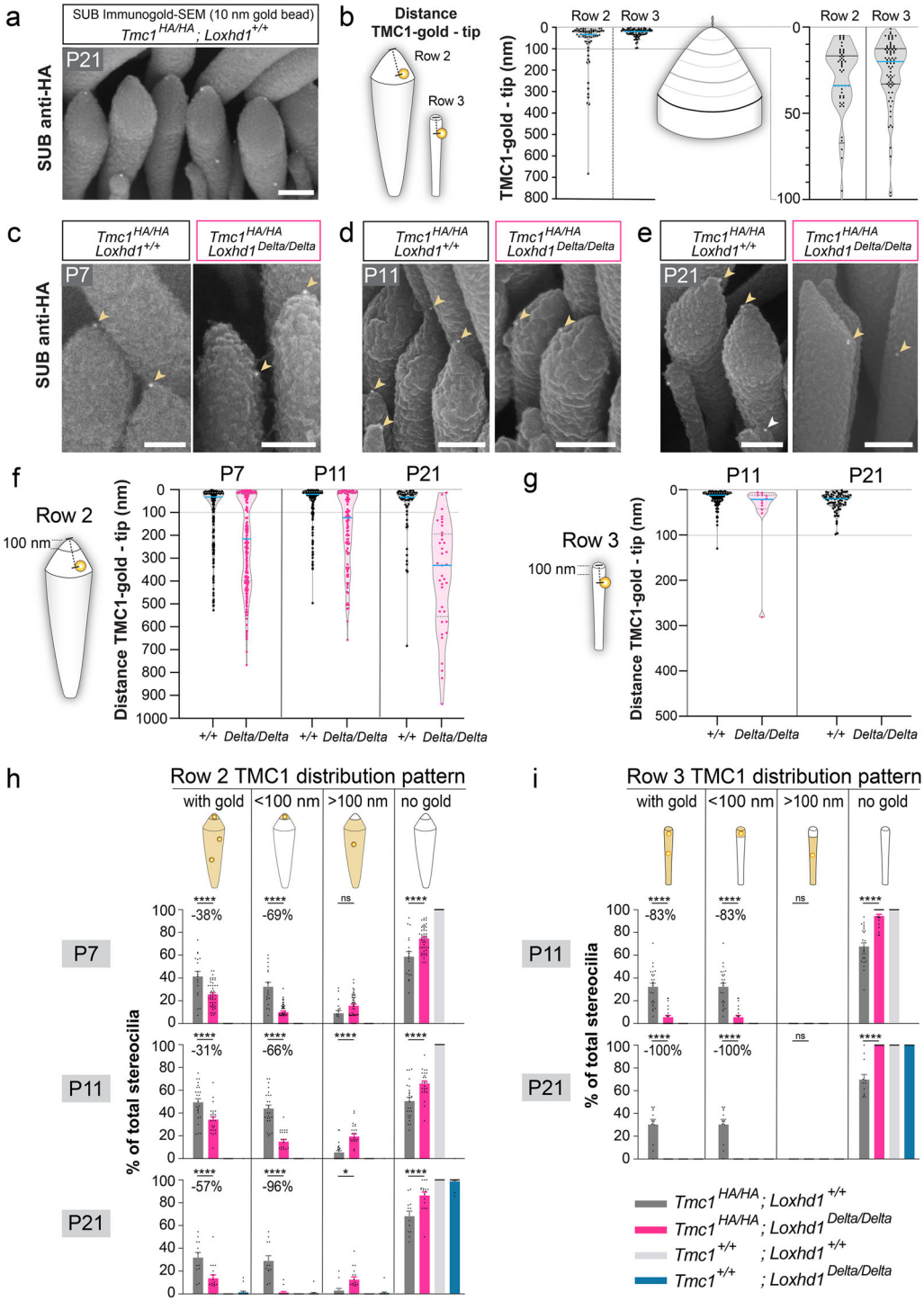

Fig. 4 | TMC1 is progressively mislocalized away from the first 100 nm of row 2 stereocilia tips of IHCs in the absence of LOXHD1. a Sub-membranous (or SUB) immunogold-SEM anti-HA with a secondary antibody conjugated to 10 nm gold-beads localizes TMC1 at the tip of rows 2 and 3 stereocilia of P21 IHCs. Note that some row 3 stereocilia were disconnected from row 2, while gold-beads were attached to row 2 shafts at the presumptive upper tip link insertion position. Scale bar = 200 nm. **b** Distance between TMC1-gold beads to the stereocilia tip in rows 2 and 3 stereocilia measured from SUB-immunogold-SEM micrographs in *Loxhd1*$^{+/+}$ IHCs. TMC1-gold beads were concentrated within 100 nm from the stereocilia tips (see the focused panel). Medians were indicated by a blue line. P21: $n_{cells} = 13$; row 2: $n_{stereocilia} = 40$; row 3: $n_{stereocilia} = 45$. **c**–**e** SUB-immunogold-SEM anti-HA detects TMC1-associated gold beads (arrowheads) at IHC row 2 tips of *Loxhd1*$^{+/+}$ and *Loxhd1*$^{Delta/Delta}$ at P7, P11, and P21. Scale bar = 200 nm. The experiment was performed once at each age. Distance between TMC1-gold beads to the stereocilia tip in row 2 (**f**) and row 3 (**g**) stereocilia measured from SUB-immunogold-SEM micrographs in *Loxhd1*$^{+/+}$ and *Loxhd1*$^{Delta/Delta}$ IHCs. Row 2: Per group: P7: $n_{cells} \geq 18$; $n_{stereocilia} \geq 113$; P11: $n_{cells} \geq 16$; $n_{stereocilia} \geq 51$; P21: $n_{cells} \geq 13$; $n_{stereocilia} \geq 30$. Row 3: P11: $n_{cells} \geq 14$; $n_{stereocilia} = 117$ for *Loxhd1*$^{+/+}$ and 12 for *Loxhd1*$^{Delta/Delta}$; P21: $n_{stereocilia} = 45$ for *Loxhd1*$^{+/+}$ and 0 for *Loxhd1*$^{Delta/Delta}$. Medians were indicated by a blue line. The experiment was performed once at each age. **h**, **i** Stereocilia classification based on the TMC1-gold distribution pattern (with at least one gold bead present regardless of its position, with at least one gold bead in the first 100 nm, with at least one gold bead below 100 nm, and without any gold beads). Row 2 (**h**): per group: P7: $n_{cells} \geq 16$; P11-P21: $n_{cells} \geq 12$; row 3 (**i**): per group: P11: $n_{cells} \geq 13$; P21: $n_{cells} \geq 11$. Represented as mean % ± SEM. Two-way ANOVA followed by Tukey's multiple comparisons tests. For all experiments. ns (non significative) = $p > 0.05$; *$p \leq 0.05$; ** $p \leq 0.01$; ***$p \leq 0.001$; ****$p \leq 0.0001$. The exact p values are presented in Supplementary Table 1. Source data are provided as a Source Data file.

($n_{cells} \geq 12$ per group, at all ages tested, Two-way ANOVA ****$p < 0.0001$, followed by Tukey's multiple comparisons test *Loxhd1*$^{+/+}$ vs. *Loxhd1*$^{Delta/Delta}$ ****$p < 0.0001$). The proportion of stereocilia with TMC1-gold beads in the first 100 nm decreased even more by 69% at P7, by 66% at P11, and by 96% at P21 (at all ages tested, Tukey's multiple comparisons test *Loxhd1*$^{+/+}$ vs. *Loxhd1*$^{Delta/Delta}$ ****$p < 0.0001$). Concurrently, the proportion of stereocilia with gold lower than 100 nm from the tip increased significantly at P11 and P21, consistent with TMC1 mislocalization (Tukey's multiple comparisons test *Loxhd1*$^{+/+}$ vs. *Loxhd1*$^{Delta/Delta}$: P7: $p = 0.085$; P11: ****$p < 0.0001$; P21: *$p = 0.0153$). When performed on row 3, this classification analysis showed a massive reduction of stereocilia with TMC1-gold beads (83% decrease at P11 and 100% decrease at P21), with the remaining TMC1 beads localizing in the first 100 nm (Fig. 4i) (P11 and P21: $n_{cells} \geq 12$ per group, Two-way ANOVA F (2, 232): ****$p < 0.0001$ and P21 F (3, 200): ****$p < 0.0001$, followed by the Tukey multiple comparisons test; *Loxhd1*$^{Delta/+}$ vs. $^{+/+}$ P11 and P21: "with gold" and "with gold <100 nm" ****$p < 0.0001$). Critically, in hair cells from our negative control animals without the *Tmc1*^{HA} allele (*Tmc1*$^{+/+}$), either *Loxhd1*$^{+/+}$ or *Loxhd1*$^{Delta/Delta}$, virtually no gold was found in stereocilia in any experiments (Fig. 4h, i), indicating that the antibody was specific for the HA-tag, at least in stereocilia.

Overall, these SUB-immunogold-SEM experiments support that LOXHD1 is required for the maintenance of TMC1 in IHC stereocilia. Importantly, LOXHD1 is also critical for maintenance of TMC1 within the first 100 nm of the row 2 tips, where the tip links insert and where the mechanical stimuli are received.

The absence of LOXHD1 leads to TMC1 mislocalization in OHCs

As LOXHD1 and TMC1 were co-expressed in OHCs, we tested if TMC1 hair bundle localization in OHCs was also affected by the *Loxhd1*^{Delta} allele, focusing on P7. We measured TMC1 fluorescence intensity in P7 OHC whole hair bundles at apical, medial, and basal positions using the *Tmc1*^{HA} allele (Fig. 5a). In wild-type mice, basal OHC hair bundles showed 2.3 times more signal than the apical ones (Fig. 5b). In the *Loxhd1*$^{Delta/Delta}$ hair bundles, the TMC1 signal exhibited a reduction across all tonotopic positions, with a more pronounced decrease at the base (−61%). Despite this reduction, TMC1 expression remained notably higher at the base than at the apex, maintaining a level 1.5 times greater ($n_{cells} \geq 27$ per group, two-way ANOVA F (2, 288) ****$p_{Genotype} < 0.0001$, ****$p_{Position} < 0.0001$, and Tukey's multiple comparisons test, *Loxhd1*$^{Delta/Delta}$ vs. $^{+/+}$: Apical: **$p = 0.0019$; Medial and Basal: ****$p < 0.0001$). Importantly, the TMC1 hair bundle signal was also found to be reduced in heterozygous *Loxhd1*$^{Delta/+}$ basal OHCs (−21%) compared with the wild-type littermates (Fig. 5b)(*Loxhd1*$^{Delta/+}$ vs. $^{+/+}$: Apical: $p = 0.9447$; Medial: $p = 0.1938$; Basal: ****$p < 0.0001$). To assess how *Loxhd1* alleles affected TMC1 stereocilia localization in OHCs, we used SUB-immunogold-SEM on OHCs (Fig. 5c). In wild-type P7 OHCs, the TMC1-gold beads were enriched in the first 100 nm from row 2 and 3 tips (73% and 97% of all beads, respectively), next to the tip links (Supplementary Fig. 6). In the *Loxhd1*$^{Delta/Delta}$ littermates, TMC1 was comparably enriched at row 2 tips (66%) but reduced at row 3 tips (62%) (Fig. 5d). In the absence of LOXHD1, the number of stereocilia with TMC1 was reduced in row 2 (−53%) and more drastically in row 3 (−69%)($n_{cells} \geq 33$ per group, Two-way ANOVA ****$p < 0.0001$, followed by Tukey's multiple comparisons test *Loxhd1*$^{+/+}$ vs. *Loxhd1*$^{Delta/Delta}$ ****$p < 0.0001$). TMC1 was also found mislocalized from the first 100 nm of row 2 (−62%) and row 3 (−80%) tips (Fig. 5e, f)(Tukey's multiple comparisons test *Loxhd1*$^{+/+}$ vs. *Loxhd1*$^{Delta/Delta}$ ****$p < 0.0001$). Therefore, as for IHCs, OHCs without LOXHD1 protein also exhibit TMC1 mislocalization in transducing stereocilia at P7.

The absence of LOXHD1 leads to BAIAP2L2 mislocalization

In P21 *Loxhd1*$^{Delta/Delta}$ IHCs, TMC1 molecules were not confined to stereocilia tips and could instead be found mislocalized along stereocilia shafts. To confirm this striking result, we investigated the localization of BAIAP2L2 protein in stereocilia. BAIAP2L2 is a member of the membrane binding I-BAR protein family and localizes at and slightly below transducing stereocilia tips[52]. The maintenance of BAIAP2L2 localization at the stereocilia tips requires the presence of MET channels and is abolished by channel blockage[52]. We therefore predicted that BAIAP2L2 molecules should follow TMC1 mislocalization in the absence of LOXHD1. By previous reports[52–54], our P21 IHC immunofluorescence staining in the control animals with a validated BAIAP2L2 antibody showed strong punctiform staining at the tips of row 2 and likely row 3 stereocilia, while BAIAP2L2 staining was instead sparse and not spatially restricted in IHCs from the *Tmc1*$^{KO/KO}$ and *Tmie*$^{KO/KO}$ mice (Fig. 6a). However, the BAIAP2L2 staining pattern in *Loxhd1*$^{Delta/Delta}$ IHCs differed from these MET channel complex mutants. First, some strong staining was still detected in row 2 stereocilia, but the proportion of stereocilia with a stained tip was drastically reduced (Fig. 6a, b) ($n_{cells} \geq 8$, Mann-Whitney test, two-tailed; ****$p_{Tip} < 0.0001$, $p_{Tip\ \&\ Shaft} = 0.6093$, ****$p_{Shaft} < 0.0001$, ****$p_{No\ signal} = 0.0006$). Second, BAIAP2L2 staining could be found ectopically along stereocilia shafts (Fig. 6a, b). To inspect nanoscale BAIAP2L2 stereocilia distribution, we performed SUB-immunogold-SEM (Fig. 6c). In P21 control (*Loxhd1*$^{+/+}$) IHCs, the BAIAP2L2-gold beads were enriched within the first 100 nm from the tip (57% for row 2 and 98% for row 3) and found below the first 100 nm to a lesser degree in row 2 (Fig. 6c–e). Within the first 100 nm, BAIAP2L2 showed a bell-shaped distribution centered at 35 nm from row 2 tips and at 30 nm for row 3 tips (Fig. 6c–e). BAIAP2L2's distribution in transducing stereocilia matched TMC1's enrichment within the first 100 nm from stereocilia tips, with the difference being that TMC1 was asymmetrically distributed in this zone, found highest at the tip and reduced after the first 50 nm (Fig. 4b, right). In P21 IHCs without LOXHD1 (*Loxhd1*$^{Delta/Delta}$), BAIAP2L2 was no longer enriched within the first 100 nm of row 2 tips (21%), but instead distributed broadly within the first micron below the tip and almost absent from row 3 (Fig. 6d, e). The proportion of row 2 stereocilia with the BAIAP2L2-gold beads within the first 100 nm was drastically reduced (−69%), and the gold beads were largely redistributed below this region (Fig. 6f)($n_{cells} \geq 33$ per group, $n_{total\ stereocilia} \geq 289$ per group; Mann-Whitney test, two-tailed, "gold <100 nm" and "gold >100 nm": ****$p < 0.0001$). Meanwhile, the proportion of row 3 stereocilia with the BAIAP2L2-gold beads was reduced by 94% (Fig. 6g). ($n_{cells} \geq 32$ per group, *Loxhd1*$^{+/+}$ $n_{total\ stereocilia} = 280$, *Loxhd1*$^{Delta/Delta}$ $n_{total\ stereocilia} = 70$; Mann-Whitney test, two-tailed, "gold <100 nm" ****$p < 0.0001$).

Overall, we conclude that in the absence of LOXHD1, BAIAP2L2 is maintained at high levels in stereocilia but relocated away from the stereocilia tips, paralleling TMC1's mislocalization.

LOXHD1 interacts in vitro with TMC1 but not with TMC2

We next wanted to understand the molecular mechanism by which LOXHD1 could facilitate the proper localization of TMC1 at the stereocilia tip. The selective effect of LOXHD1 on the localization of TMC1, while not impacting TMC2 or LHFPL5, and only partially affecting TMIE (Fig. 3 and Supplementary Fig. 4) suggests that mislocalization is unlikely to be due to a general effect. Hence, we tested whether LOXHD1 could interact physically with TMC1 but not with TMC2 despite their strong homology (58% aa identity and 74% aa similarity). To test protein–protein interactions, we employed biochemistry. We single or co-transfected HEK293T cells with tagged full-length LOXHD1 and tagged candidate interactor constructs. After 48 hours of culture, the cell extracts were subjected to immunoprecipitation with anti-tag antibodies, subsequently run on SDS-PAGE gels and analyzed with tag-specific antibodies on western blots (co-immunoprecipitation assay or Co-IP). When FLAG-TMC1 or FLAG-TMC2 was co-expressed with LOXHD1-HA and protein extracts subjected to pull down by the HA-tag on LOXHD1, TMC1 was co-immunoprecipitated, whereas TMC2 was not (Fig. 7a and Supplementary Fig. 7a). The TMC1 interaction with LOXHD1 was further confirmed when FLAG-TMC1 was

https://doi.org/10.1038/s41467-024-51850-4

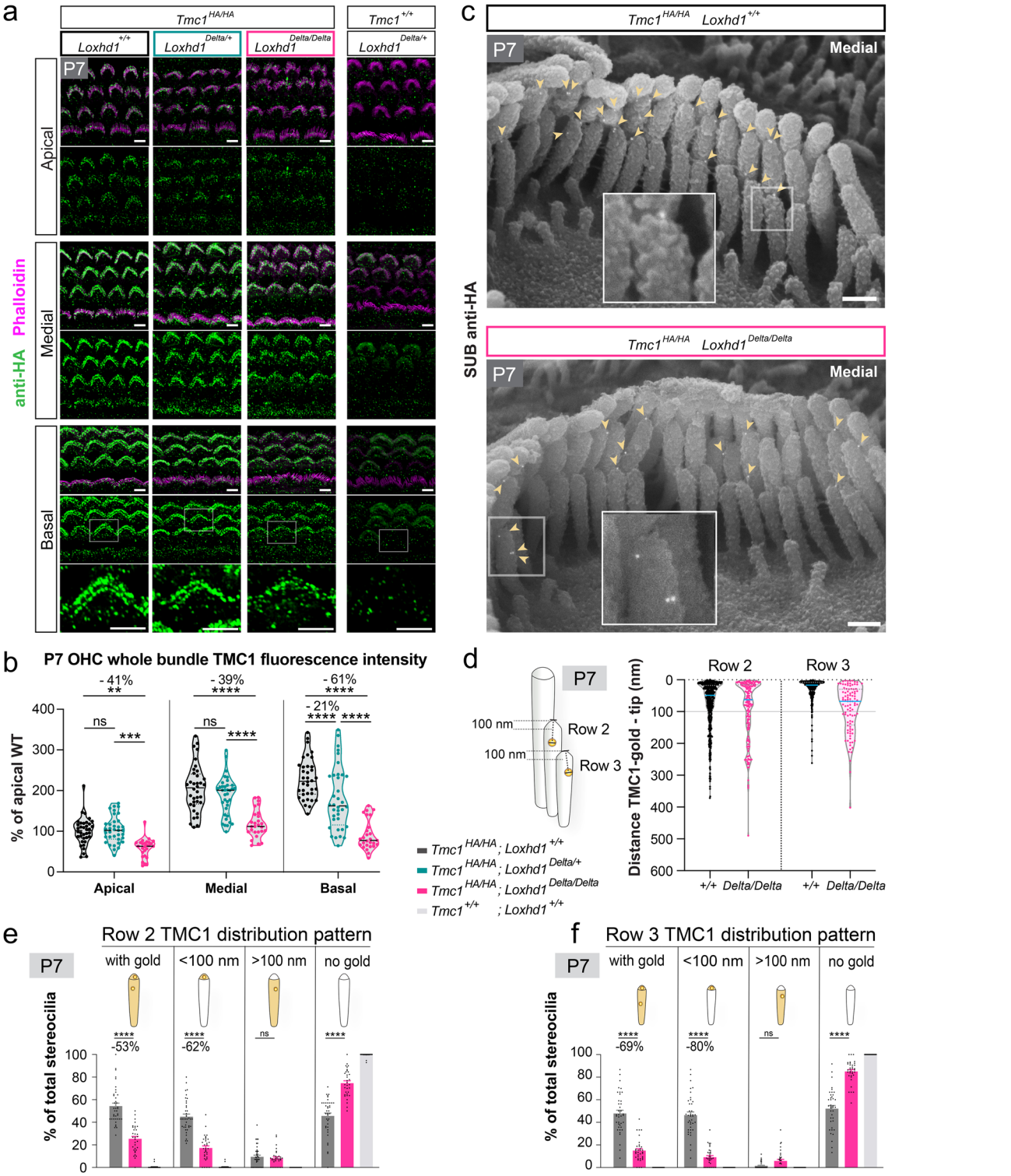

Fig. 5 | TMC1 localization in OHC stereocilia is affected by the *Loxhd1*^{Delta} allele. **a** TMC1 localization by immunofluorescence (anti-HA) in P7 OHC hair bundles (Phalloidin) along the tonotopical axis in *Tmc1*$^{HA/HA}$ with *Loxhd1*$^{+/+}$, *Loxhd1*$^{Delta/+}$, or *Loxhd1*$^{Delta/Delta}$. *TMC1*$^{+/+}$; *Loxhd1*$^{Delta/+}$ was used as "non-HA" negative control. Scale bars = 4 μm. **b** Whole hair bundle TMC1-HA fluorescence intensity quantification on P7 apical, medial, and basal OHCs of *Tmc1*$^{HA/HA}$ with *Loxhd1*$^{+/+}$, *Loxhd1*$^{Delta/+}$, or *Loxhd1*$^{Delta/Delta}$ animals. Then intensity values were normalized to the mean fluorescence intensity of apical *Tmc1*$^{HA/HA}$; *Loxhd1*$^{+/+}$ OHCs. Per group: $n_{cells} \geq 27$. The experiment was replicated twice. Two-way ANOVA followed the Tukey test. **c** SUB-immunogold-SEM anti-HA detects TMC1-associated gold beads (10 nm, arrowheads) at OHC row 2 and 3 tips of *Loxhd1*$^{+/+}$ and *Loxhd1*$^{Delta/Delta}$ P7 medial OHCs. The experiment was performed once. Scale bars = 200 nm. **d** Distance between TMC1-gold beads to the stereocilia tips in row 2 and 3 stereocilia measured from SUB-immunogold-SEM micrographs in *Loxhd1*$^{+/+}$ and *Loxhd1*$^{Delta/Delta}$ P7 OHCs. Quantified OHCs were from pooled tonotopic positions distributed as follow: 35% apical, 27% middle, and 38% basal. Per group: P7 row 2: $n_{cells} \geq 38$; $n_{stereocilia} \geq 113$; row 3: $n_{cells} \geq 39$; $n_{stereocilia} \geq 75$; The experiment was performed once. **e**, **f** Stereocilia classification based on the TMC1-gold distribution pattern: with at least one gold bead present regardless of its position, with at least one gold bead in the first 100 nm, with at least one gold bead below 100 nm, and without any gold beads. Row 2 (**e**): per group: $n_{cells} \geq 33$; row 3 (**f**): per group: $n_{cells} \geq 35$; Represented as mean % ± SEM. Two-way ANOVA followed by Tukey's multiple comparisons tests. For all experiments. ns (non significative) = $p > 0.05$; *$p \leq 0.05$; **$p \leq 0.01$; ***$p \leq 0.001$; ****$p \leq 0.0001$. The exact p values are presented in Supplementary Table 1. Source data are provided as a Source Data file.

https://doi.org/10.1038/s41467-024-51850-4

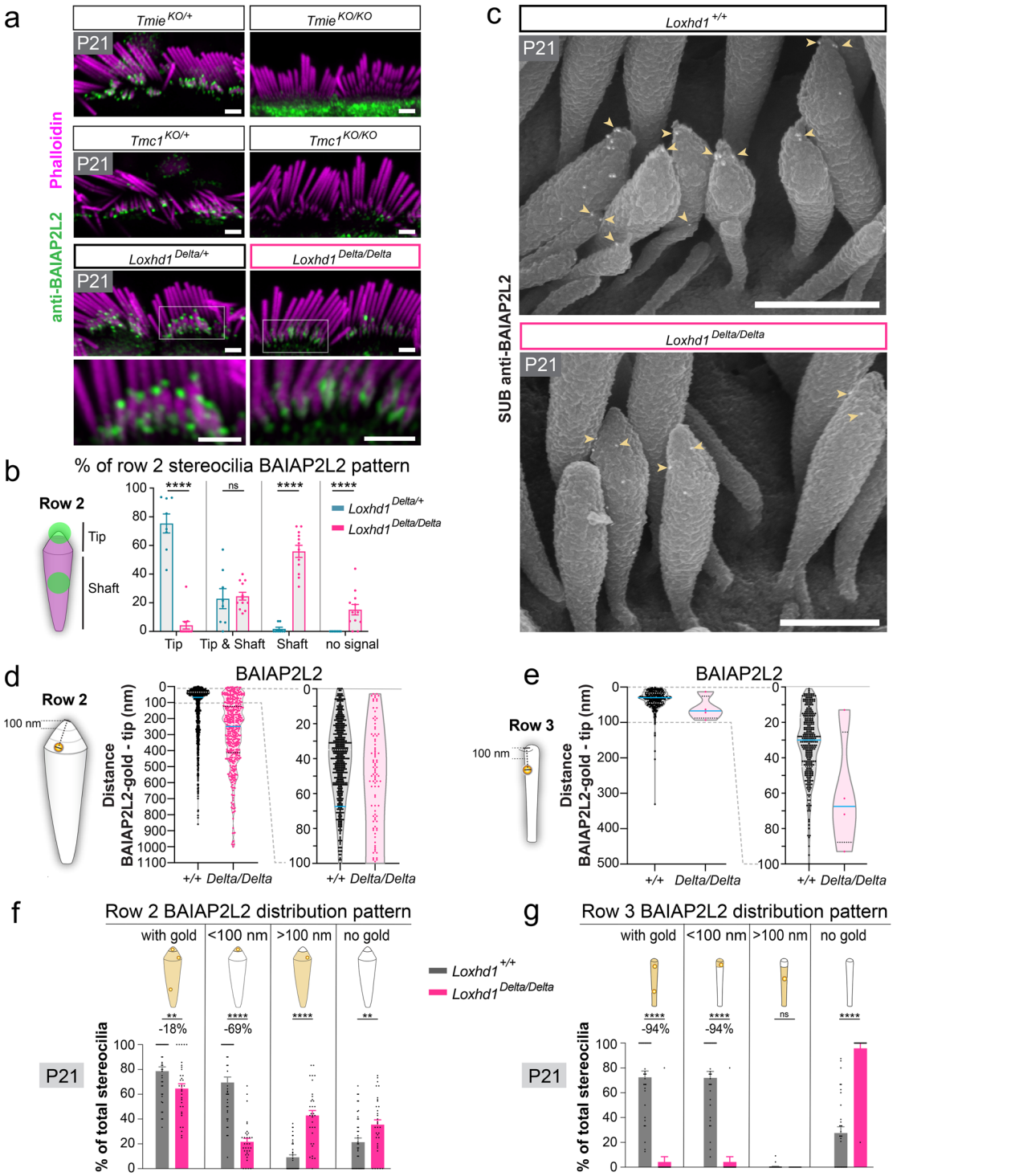

Fig. 6 | The absence of LOXHD1 leads to BAIAP2L2 mislocalization. a Anti-BAIAP2L2 immunofluorescence on P21 apical HCs shows a strong signal at transducing stereocilia tips which is absent in the mechanotransduction deficient IHC mutants *Tmie*$^{KO/KO}$ and *Tmc1*$^{KO/KO}$. In *Loxhd1*$^{Delta/Delta}$, a strong BAIAP2L2 signal is detected in row 2 stereocilia but with a different distribution than control *Loxhd1*$^{Delta/+}$ littermates. Boxes correspond to magnified panels. Scale bars = 2 µm. Representative results from experiments replicated once (*Tmie*^{KO}) or twice (*Tmc1*^{KO} and *Loxhd1*^{Delta}). **b** Stereocilia classification based on the BAIAP2L2 fluorescence signal distribution pattern: only at the tip, at both the tip and along the shaft, at the shaft, or absent from stereocilia. Data are represented as mean ± SEM. The experiment was replicated twice. Per group: $n_{cells} \geq 8$; Mann–Whitney test, two-tailed. **c** SUB-immunogold-SEM anti-BAIAP2L2 shows the enrichment of gold beads at the tip of rows 2 and 3 P21 IHC stereocilia in *Loxhd1*$^{+/+}$, while gold beads were more distant from the tip in *Loxhd1*$^{Delta/Delta}$. Arrowheads indicate the gold beads closest to the tips. Scale bars = 500 nm. Distance between BAIAP2L2-gold beads to tip of rows 2 (**d**) and 3 (**e**) stereocilia measured from SUB-immunogold-SEM micrographs in *Loxhd1*$^{+/+}$ and *Loxhd1*$^{Delta/Delta}$ P21. IHCs corresponded to ~70% apical, ~12% medial, and ~18% basal. Per group: P21 row 2 (**d**) $n_{cells} \geq 34$; $n_{stereocilia} \geq 168$; row 3 (**e**) $n_{cells} \geq 34$; $n_{stereocilia} = 155$ for *Loxhd1*$^{+/+}$ and 4 for *Loxhd1*$^{Delta/Delta}$; The experiment was replicated twice. Stereocilia classification based on the BAIAP2L2-gold distribution pattern: with at least one gold bead present regardless of its position, with at least one gold bead in the first 100 nm, with at least one gold bead below 100 nm, and without any gold beads. Represented as mean % ± SEM. Row 2 (**f**): per group: $n_{cells} \geq 33$; row 3 (**g**): per group: $n_{cells} = 32$. Mann-Whitney test, two-tailed. For all experiments. ns (non significative) = $p > 0.05$; *$p \leq 0.05$; **$p \leq 0.01$; ***$p \leq 0.001$; ****$p \leq 0.0001$. The exact p values are presented in Supplementary Table 1. Source data are provided as a Source Data file.

https://doi.org/10.1038/s41467-024-51850-4

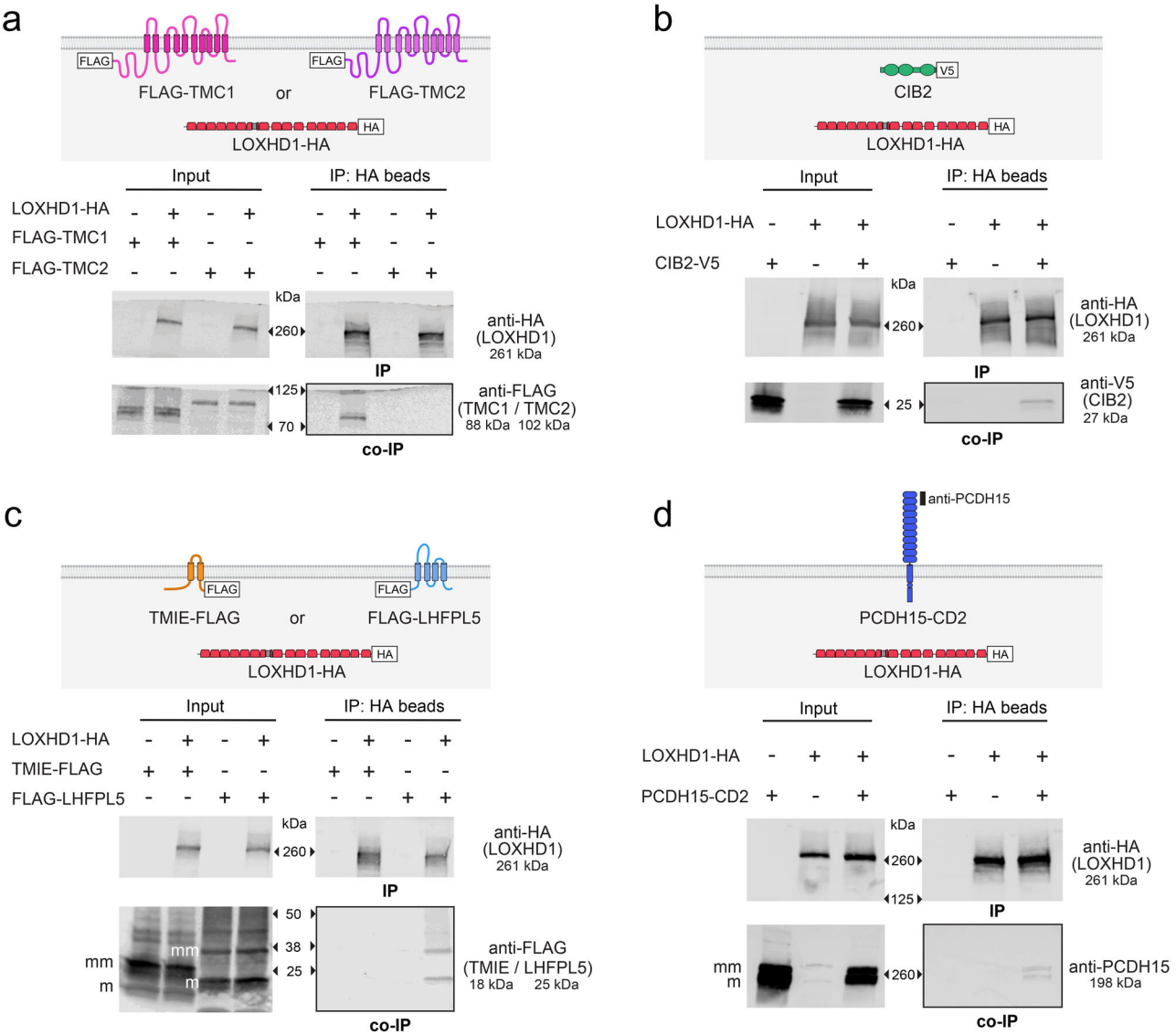

Fig. 7 | LOXHD1 interacts in vitro with MET channel complex and tip link proteins. a–d Co-immunoprecipitation experiments from HEK293T cells over-expressing LOXHD1-HA with tagged channel complex or tip link proteins. FLAG-TMC1 was co-immunoprecipitated with LOXHD1-HA using anti-HA magnetic beads, but FLAG-TMC2 was not (**a**); CIB2-V5 (**b**), FLAG-LHFPL5 (**c**) and PCDH15 (**d**) were co-immunoprecipitated with LOXHD1-HA, while TMIE-FLAG was not (**b**). Each experiment was replicated at least thrice; (**a**) was replicated five times. Predicted protein sizes based on primary sequence: LOXHD1-HA: 261 kDa; TMC1-FLAG: 88 kDa; TMC2-FLAG: 102 kDa; CIB2-V5: 27 kDa; HA-CIB2: 23 kDa; TMIE-FLAG: 18 kDa; FLAG-LHFPL5: 25 kDa; PCDH15: 198 kDa. m: monomeric protein molecular size; mm: multimeric molecular size; IP: Immunoprecipitation. For corresponding full blots, see Supplementary Fig. 7.

immunoprecipitated by the FLAG antibody (Supplementary Fig. 8a). These experiments demonstrate that LOXHD1 interacts selectively in vitro with TMC1 but not with TMC2.

LOXHD1 interacts in vitro with CIB2 but not with TMIE

Next, we similarly tested whether LOXHD1 could interact with other known MET channel complex components CIB2 and TMIE, both of which are required for the presence and function of TMC1 in the hair bundle[7,9–13,32]. When LOXHD1-HA and CIB2-V5 were co-expressed and protein extracts pulled down by LOXHD1-HA, CIB2 was co-immunoprecipitated (Fig. 7b and Supplementary Fig. 7b). Conversely, when the immunoprecipitation was done with the HA-antibody against CIB2-HA probing for an interaction with LOXHD1-MYC, LOXHD1 was co-immunoprecipitated with CIB2, providing additional evidence for the interaction (Supplementary Fig. 8b). Contrarily, when FLAG-TMIE was co-expressed with LOXHD1-HA, TMIE did not co-immunoprecipitate along with LOXHD1 (Fig. 7c and Supplementary Fig. 7c). The data demonstrate that LOXHD1 interacts in vitro with CIB2 but not with TMIE.

LOXHD1 interacts in vitro with LHFPL5 and the lower tip-link protein PCDH15

We found that LOXHD1 can interact with the MET channel complex proteins TMC1 and CIB2, but not with TMC2 or TMIE. We next wanted to test whether LOXHD1 could also interact with LHFPL5, proposed as contributing to force transmission from the tip link to the MET channel and can itself bind to TMC1 and TMIE and the tip link protein PCDH15[12,14,15,19]. When LHFPL5-FLAG was co-expressed with LOXHD1-HA in HEK293T cells and protein extracts were subjected to immunoprecipitation with the HA antibody, LHFPL5 was co-immunoprecipitated with LOXHD1 (Fig. 7c and Supplementary Fig. 7c). Conversely, LOXHD1 co-immunoprecipitated

https://doi.org/10.1038/s41467-024-51850-4

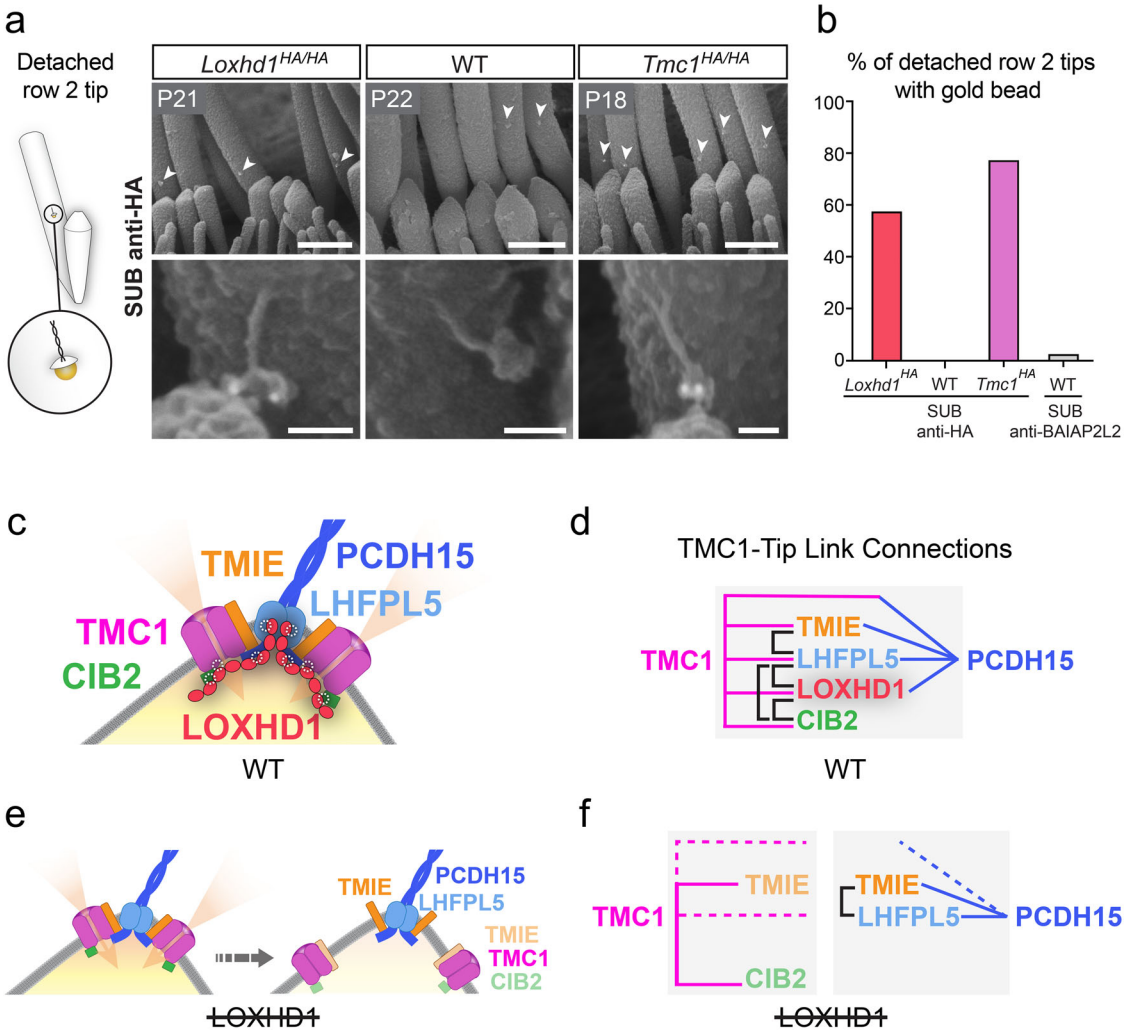

Fig. 8 | LOXHD1 and TMC1 are part of protein complexes attached to the tip-link branches in vivo, and molecular interaction models between TMC1 and the tip link, with or without LOXHD1. a In SUB experiments on P21 IHCs, some row 2 tips are detached from the rest of the stereocilia but still connected to the tip links (arrowheads and high magnification in the lower panels). Anti-HA gold-beads were specifically found at detached row 2 tips for LOXHD1-HA and TMC1-HA but not in the WT sample. Scale bars: 500 nm and 50 nm for the low and high mag pictures, respectively. **b** Quantification of the percentage of P21 IHC detached row 2 tips containing gold. *Loxhd1*$^{HA/HA}$ anti-HA: $n_{cells} = 17$, $n_{detached\ tip\ with\ gold\ /\ total} = 31/54$; WT anti-HA: $n_{cells} = 5$, $n_{detached\ tip\ with\ gold\ /\ total} = 0/11$; *Tmc1*$^{HA/HA}$ anti HA: $n_{cells} = 10$, $n_{detached\ tip\ with\ gold\ /\ total} = 34/44$; WT anti-BAIAP2L2: $n_{cells} = 14$, $n_{detached\ tip\ with\ gold\ /\ total} = 1/42$. The experiment was performed once. **c** Cartoon representing the mature auditory mechanotransduction protein complex in the wild-type (WT). **d** Model summarizing the molecular connections between TMC1 and PCDH15. **e** Cartoon representing the mature auditory mechanotransduction protein complexes in the absence of LOXHD1: initially, a population of TMC1 channels still functions while a second population, progressively increasing in proportion, is physically disconnected from the tip-link and cannot receive sound-induced forces. **f** Model summarizing the molecular connections between TMC1 and PCDH15 persisting upon the absence of LOXHD1: some TMC1/LHFPL5/TMIE proteins are initially sufficient to maintain some TMC1 channels at the tip link. However, with time, more and more TMC1 is found at a distance from the PCDH15, with LHFPL5 remaining attached to PCDH15 along with some TMIE molecules. A subset of TMIE proteins is predicted to remained attached to the mislocalized TMC1 molecules. The predicted localization of CIB2 remains hypothetical. However, considering that CIB2 can interact with BAIAP2L2 and is necessary for proper localization of BAIAP2L2 in hair bundles[54], and given that we observed BAIAP2L2 mislocalization similar to TMC1 at P21, it is probable that CIB2 is also associated with the mislocalized TMC1 molecules and absent from the stereocilia tip. Predicted positions are indicated with transparent colors. Source data are provided as a Source Data file.

along with FLAG-LHFPL5, confirming their interaction (Supplementary Fig. 8a). Finally, we wondered whether LOXHD1 could interact with the lower tip-link protein PCDH15. We focused on PCDH15-CD2, the only PCDH15 isoform indispensable for hearing in mice[55,56]. When PCDH15-CD2 was co-expressed with LOXHD1-HA and cell extracts subjected to anti-HA pulldown, PCDH15 was co-immunoprecipitated with LOXHD1 (Fig. 7d and Supplementary Fig. 7d). The interaction was also confirmed upon PCDH15 immunoprecipitation (Supplementary Fig. 8c).

In conclusion, LOXHD1 interacts selectively with three of the five known MET channel complex proteins TMC1, CIB2, and LHFPL5 plus the lower-tip link protein PCDH15 (Fig. 8a, b).

LOXHD1 and TMC1 proteins are part of complexes attached to the tip-link in vivo

Interestingly, in the P21 IHC preparation that underwent SUB-immunogold-SEM, we noted that tip links joining rows 1 and 2 of IHCs were often detached at their lower insertion side but remained attached at their upper side to the tallest stereocilia (Fig. 8a). Extra material from the tips of row 2 was consistently connected to the tip links, indicating that the breaking points were located deeper than the site of lower tip-link membrane insertion. When anti-HA SUB-immunogold-SEM was performed on hair cells from *Loxhd1*$^{HA/HA}$ mice, LOXHD1-gold beads were frequently found attached to this externalized lower tip-link insertion material (57% of detached row 2 tips) (Fig. 8a, b). LOXHD1-

gold beads appeared positioned below each tip link branch (Fig. 8a). Conversely when the experiment was performed on non-HA animals, no gold was detected on the detached lower tip-link insertion material (Fig. 8a, b). When anti-HA SUB-immunogold-SEM was done on hair cells from *Tmc1*$^{HA/HA}$ mice, the gold beads were also frequently attached (77%) (Fig. 8a, b and Supplementary Fig. 9a). This result demonstrates that TMC1 channel complexes are physically connected to the tip link. By contrast, when anti-BAIAP2L2 SUB was performed on the P21 wild-type animals, the gold beads were rarely found (2%) at the detached row 2 tips (Fig. 8b and Supplementary Fig. 9b). Thus, we conclude that as for TMC1, LOXHD1 proteins are integral to protein complexes attached to the lower tip-link branches in vivo.

In summary, LOXHD1 acts as a molecular hub with the ability to interact with proteins from both the tip link and the MET channel complex. LOXHD1 plays a unique and indispensable role in maintaining TMC1 molecules at this nanometric site of the stereocilia membrane. Without LOXHD1, TMC1 molecules become progressively mislocalized, preventing their directional mechanical activation by sound-induced forces (Fig. 8c, d). This phenotype represents a novel molecular mechanism causing hearing loss in vertebrates.

Discussion

Here, we demonstrate the existence of an unanticipated critical element of the mature vertebrate auditory MET machinery: an internal molecular hub localized at the tip of transducing stereocilia. This element, LOXHD1, is capable of binding in vitro to the lower tip-link protein as well as three out of the four proteins that make up the auditory ion channel complex. Without LOXHD1, the MET channel subunit TMC1 is progressively not maintained at the tip link. As a consequence of this mislocalization, force transmission from the tip link to the distant MET channel is impaired; therefore, the auditory MET channels including TMC1 cannot be activated by sound-induced forces, leading to hearing loss.

TMC1 MET is selectively affected by the absence of LOXHD1

We found that two phenotypes occur in cochlear hair cells without LOXHD1.

First, the quantities of TMC1 molecules were progressively reduced in stereocilia, suggesting that LOXHD1 is not indispensable for the initial presence of TMC1 in the stereocilia like the other MET complex proteins CIB2, TMIE, or LHFPL5[10,13,14,32]. Instead, we found that LOXHD1 is necessary for the maintenance of TMC1 in stereocilia. The depletion of TMC1 molecules within stereocilia significantly affects row 3 of IHCs and OHCs homozygous *Loxhd1*$^{Delta/Delta}$, which precedes the onset of morphological defects in stereocilia width and maintenance. Importantly, while TMC1 expression is not affected in heterozygous *Loxhd1*$^{Delta/+}$ IHCs at P21, it is reduced in OHCs already at P7, likely explaining the partial hearing loss of the heterozygous animals.

Second, in the absence of LOXHD1, the remaining TMC1 molecules progressively lose their stereocilia tip enrichment, creating a mismatch between potentially mechanically activatable TMC1 channels and the tip-link insertion points. At P7, when TMC2 is present and contributes to half of the current[16], the absence of LOXHD1 would affect only TMC1 (31% row 2 tips with TMC1 remaining) (Fig. 4h). Therefore, the predicted max MET current would be 352 pA in agreement with the measured 357 ± 54 pA (Fig. 1m, n). At P11, IHC MET currents were reduced by 84% in the absence of LOXHD1 from 412 ± 60 pA to 66 ± 46 pA (Fig. 1o, p). If we consider that rows 2 and 3 contribute equally to these currents[28], then we would predict that in the absence of LOXHD1, 34% of row 2 tips and 17% of row 3 tips with TMC1 would generate a total of 105 pA of MET maximum currents (Fig. 4h, i). This prediction aligns with the mean of the measured current, falling within one standard deviation. Therefore, the decrease in the number of transducing stereocilia with TMC1 at their tips explains the reduction of MET current. At P21, based on TMC1 SUB-immunogold-SEM localization, only 2% of the MET current would be left, preventing hair cell depolarization by sound and leading to hearing loss. Overall, in the absence of LOXHD1, the MET currents of channels containing TMC1 were affected, while those containing TMC2 seem not to be. These results are supported by the fact that the proportion of row 2 tips with TMC2 is unaffected in *Loxhd1*$^{Delta/Delta}$ (Fig. 3c, d) and that TMC2 cannot bind LOXHD1 in vitro (Fig. 7a). This later result is striking as both proteins are closely related. This suggests also that TMC2 molecules are not maintained at the tip of transducing stereocilia through the same molecular mechanism required for TMC1. It will be important to assess whether the distribution of TMC2 at the stereocilia tip mirrors that of TMC1 or not. TMC2 may exhibit a broader distribution than TMC1 at the stereocilia tip and might not necessitate a direct interaction with the tip link for its activation. Alternatively, TMC2 maintenance at the tip link could necessitate only direct interaction with PCDH15 or it could be mediated by TMIE or by an unidentified molecule fulfilling the role of LOXHD1 for TMC2. These inquiries will be investigated in following studies.

Overall, LOXHD1 is an additional component of the auditory MET machinery, which is exclusive to a given TMC paralogue, implying that further differences could exist between the TMC1 and TMC2 channels, such as distinct interactions with the cytoskeleton, tip link, or membrane, and that these distinct channels could potentially have different channel gating mechanisms and activity regulations as well.

The mature auditory MET channel complex requires an additional component to maintain connectivity to the tip link

Previous in vitro and electrophysiological studies have reported the existence of three molecular interactions between the pore channel subunit TMC1 and the lower part of the tip link, PCDH15: TMC1 can interact directly with PCDH15[34], or indirectly via TMIE or LHFPL5, which can also interact between themselves (Fig. 8c, d)[12–14,32,33]. Without LOXHD1, the combination of these three connections is initially sufficient to maintain 32% of TMC1 channels connected the tip link (Fig. 8e, f). This result shows that: 1) LOXHD1 is not indispensable to establish a connection between TMC1 and the tip link, 2) the force transmission can occur at least to some degree without LOXHD1, and 3) as some TMC1/tip link connections are preserved, LOXHD1 is not positioned in series with the other connections but instead in parallel. Hence, we propose that different molecular connections between the tip link and the channel complex may serve different functions, which may not be strictly essential for the force transmission process.

Eventually, in the absence of LOXHD1, the combination of the three previously known connections is insufficient to maintain TMC1 molecules at the tip link. Therefore, LOXHD1 is indispensable for maintaining the connectivity of TMC1 to the tip link.

Interestingly, by elucidating how a specific MET complex component is influenced by the disconnection of TMC1 with PCDH15, valuable insights into the strengths of their mutual in vivo interactions can be deduced from our experiments with *Loxhd1*$^{Delta/Delta}$ mutant hair cells (Fig. 8e, f): Because LHFPL5 is maintained at the tip of stereocilia while TMC1 is mislocalized at P11, the interaction between LHFPL5-PCDH15 appears stronger than the LHFPL5-TMC1 interaction. Therefore, LHFPL5 is integral to the lower tip link, in line with previous in vitro data[15,36]. Contrarily, as TMIE is partially removed from stereocilia tips (−33%) while TMC1 is mislocalized to a great extent (−66%) at P11 in *Loxhd1*$^{Delta/Delta}$, a TMIE pool must bind equally or more strongly to TMC1 than to PCDH15 and LHFPL5.

Overall, by binding to three MET channel complex components and the tip link, we propose that LOXHD1 provides cohesiveness and stability to the channel complex–tip link connection. The interaction between LOXHD1 and PCDH15 could occur through direct binding, indirect mediation via LHFPL5, or a combination of both mechanisms. Therefore, while the multi-component nature of the MET channel complex is important for providing different modes of activity

regulations, like TMIE for PIP_2[13] and CIB2[11] for its potential interaction with cytoskeletal proteins, its multi-component nature is also a weakness. The mature MET machinery requires a dedicated mechanism to maintain the cohesion and integrity of the channel complex and its connection to the tip link to remain functional.

Besides these discoveries, our work demonstrates that auditory channels disconnected from the tip links can be maintained in the stereocilia membrane at least until P21. The preservation of TMC1 molecules within the second row of stereocilia in the absence of LOXHD1, is likely responsible for the lack of significant morphological abnormalities in these stereocilia until P21. Our findings also open the exciting possibility that the mislocalized channels could be reconnected to the tip link even at a late stage, potentially allowing for therapeutic intervention to restore MET function and hearing of the *Loxhd1*-deficient mice and, ultimately, human DFNB77 patients.

Nanoscale mapping of the auditory machinery in stereocilia

LOXHD1 and the other subunits of the MET channel complex are present at low levels in stereocilia. To track these endogenous proteins in stereocilia at nanoscale resolution, we used our recently developed SUB-immunogold-SEM method[50]. This method allows the imaging and mapping of gold bead conjugated antibodies to detect internal epitopes along cell surfaces. Most importantly, this technique permits fast sampling of large sample numbers, providing high accuracy and sensitivity to our quantifications. For instance, TMC1 distribution analysis in wild-type IHC hair bundles (P7, P11, and P21) integrated data from 56 cells, 459 stereocilia, and 646 gold beads. This method opens possibilities for hair bundle investigations from embryonic to adult stages, such as the identification of minute but functionally relevant alterations in protein localization, or in determining protein localization in small row 3 stereocilia.

In this study, we precisely mapped the position of the TMC1 subunit of the auditory MET channel complex in stereocilia. While TMC1 has been previously localized at the tip of stereocilia by fluorescence and even by immunogold-TEM microscopy, the distribution of TMC1 molecules relative to the stereocilia tip could not be measured[30,39,57]. Here, we showed that TMC1 molecules are concentrated at the extreme tip of stereocilia, contained in the first 100 nm, and concentrated further within the first 50 nm for row 2 and 3 stereocilia of IHCs and OHCs. These measurements were from fixed, dehydrated, and metal-coated samples. To convert them to living measurements, we can take advantage of the scaling factors determined in our previous study[58], giving an estimated TMC1 concentration within the first 83 nm from tips of living transducing stereocilia, so very close to the predicted insertion point of the tip link. However, a lingering question concerning the mechanical activation mechanism of the auditory channels is whether they are tethered to the tip link or if they instead float freely in the surrounding membrane adjacent to the tip-link insertion point[59–61]. Through our SUB-immunogold-SEM preparation, we observed tip links frequently detached at their lower insertion side, yet carrying some row 2 tip material containing TMC1-gold beads. These in situ observations unequivocally demonstrate that the TMC1-MET channel complexes are tethered to the tip link, either directly or indirectly, rather than floating freely in the adjacent plasma membrane.

Moreover, we found LOXHD1 to be also strongly connected to the channel complexes and the tip link in these preparations.

In conclusion, we provide strong evidence here that LOXHD1 is an integral element of the auditory MET machinery, required to maintain TMC1 at the tip-link insertion point, likely by establishing an additional molecular connection between them. LOXHD1 could have other molecular functions, such as contributing to the force transmission and modulation of auditory channel activity. These hypotheses, as well as the systematic mapping of the other MET complex subunits in stereocilia at the nanoscale with SUB-immunogold-SEM, will be explored in further studies.

Limitations of the study

Given that the best tool available to track CIB2 is an antibody that has a high background level, we could not determine with accuracy if CIB2 was affected by LOXHD1's absence. A tagged KI animal would be ideal to answer this question, but finding a location in this small protein for tag insertion and maintaining its function is challenging.

Methods

Mouse strains

The Administrative Panel on Laboratory Animal Care (APLAC) at Stanford University (APLAC protocols #28278 and #30305) approved all animal procedures. Mice of both sexes were used in all experiments. The mice were housed in standard Innovive cages with bedding (San Diego, CA) under 12 hours light/dark cycles with permanent access to food and water, with room temperature (RT) maintained at around 22 °C. The mice were also inspected weekly for any signs of discomfort, and the sentinel mice were regularly tested for infection on each cage rack.

Tmc1^{HA}, *Tmc2*^{Myc}, and *Tmie*^{HA} were obtained from Dr. Cunningham and Dr. Müller (J. Hopkins University) [13], *Tmie*^{KO}[62] (B6.B(CBA)-*Tmie*^{sr}/J, JAX 000543) from JAX, and *Tmc1*^{KO} [3] (B6.129-*Tmc1*$^{tm1.1Ajg}$/J, JAX 019146, backcrossed on C57Bl6/J) from Dr. Beurg and Dr. Fettiplace (Wisconsin-Madison University). The mice were genotyped as previously described, and the C57BL6/J wild-type mice were purchased from Charles River Laboratories.

Loxhd1^{Delta} and *Loxhd1*^{HA} mouse generation

The *Loxhd1*^{Delta} and *Loxhd1*^{HA} alleles were generated by CRISPR/Cas9 gene editing. sgRNA target sites were selected using the CRISPRscan (crisprscan.org) or CRISPick (Broad Institute) websites. For the *Loxhd1*^{Delta} allele, the original design was meant to generate a floxed allele with a direct recombination reporter (mScarlet) like the previous design[63]. An sgRNA target site located between Exon 1 (gG18NGG-64) and Exon 2 was selected to insert *LoxP/FRT* elements (Primer: T7 promoter containing forward primer for amplifying Loxhd1 5′ cutting site sgRNA template from pX461: taatacgactcactatagGCATTTCTGTCAC CGTGCTAgttttagagctagaa), and a second sgRNA target site after the last exon (Exon 41) was selected to insert *LoxP/SA/mScarlet/FRT* elements (Primer: T7 promoter containing forward primer for amplifying Loxhd1 3′ cutting site sgRNA template from pX461: taatacgactcactatagGGGCACAGGGGACACGAGGAgttttagagctagaa). sgRNAs were synthesized from DNA templates by in vitro transcription with the HiScribe T7 High Yield RNA Synthesis Kit (NEB, E2040S). Each sgRNA DNA template was produced by PCR using a specific sense primer that contains a T7 promoter and an sgRNA target sequence and an antisense primer amplification on the pX461 vector (https://www.addgene.org/48140/) that contains a common sgRNA sequence (Primer: Common reverse primer for amplifying sgRNA template from pX461: AAAAGCACCGACTCGGTGCC). Single-stranded oligodeoxynucleotides (ssODNs) for inserting desired elements were synthesized by using the Guide-it Long ssDNA Production System (Takara, 632644). A mix of the Cas9 nuclease protein (15 ng/µl, NEB, M0386S), 2 sgRNAs (15 ng/µl for each), ssODN for *LoxP/FRT* (2 ng/µl), and ssODN for *LoxP/SA/mScarlet/FRT* (8 ng/µl) diluted in nuclease-free injection buffer (10-mM Tris-Cl, 0.1-mM EDTA, pH 7.4) was used for pronuclear injection into one-cell C57BL/6 J embryos.

LoxP/FRT: ttatcactgctctttaacttcgtataaacagagtcactcgatgtgtgtttcttt gggagataagtctcactctgtggttcaggtttgtttttcttaggctatactcactgtgtagcccagg ctagtcttaaatgctcagccagaagttcctattccgaagttcctattctctagaaagtataggaact tcgtcgagataacttcgtatagcatacattatacgaagttattcctcgtgtcccctgtgcctggtgc tggcattacagggtgagctctgagttttgtggtgtgtatatatttgtgtctatcttctttcctaccac cctgcccaagagattcgtgcatggtgtaacccgaggcacagtttg

LoxP/SA/mScarlet/FRT: tcctatggaatgtatgaaagaaaagattgtacagtgatat cccatgttaaacacgttgtctcagggaactcctgggtttgggaaaggtgaacaccagaagtcct gcttcagtttataagtattcatttattgagcatctacaaagatatcttagcgaattttcttagtcacat ttctgtcaccgtgctaataacttcgtatagcatacattatacgaagttatactagtggatccctgca gatctgtagggcgcagtagtccagggtttccttgatgatgtcatacttatcctgtccctttttttcc acagctcgcggttggaggacaaactcttcgcggtctttccagtgggtgagcaagggcgaggca gtgatcaaggagttcatgcggttcaaggtgcacatggagggctccatgaacggccacgagttc gagatcgagggcgagggcgagggccgcccctacgagggcacccagaccgccaagctgaag gtgaccaagggtggccccctgcccttctcctgggacatcctgtcccctcagttcatgtacggctc cagggccttcaccaagcaccccgccgacatccccgactactataagcagtccttccccgaggg cttcaagtgggagcgcgtgatgaacttcgaggacggcggcgccgtgaccgtgacccagga cacctccctggaggacggcaccctgatctacaaggtgaagctccgcggcaccaacttcctcct gacggccccgtaatgcagaagaagacaatgggctgggaagcatccaccgagcggttgtaccc cgaggacggcgtgctgaagggcgacattaagatggccctgcgcctgaaggacggcggccgc tacctggcggacttcaagaccacctacaaggccaagaagcccgtgcagatgcccggcgcctа caacgtcgaccgcaagttggacatcacctcccacaacgaggactacaccgtggtggaacagta cgaacgctccgagggccgccactccaccggcggcatggacgagctgtacaagtaaagcggc cgcgactctagatcataatcagccataccacatttgtagaggttttacttgctttaaaaaacctccc acacctcccccgaacctgaaacataaaatgaatgcaattgttgttgttaacttgtttattgcagct tataatggttacaaataaagcaatagcatcacaaatttcacaaataaagcatttttttcactgcattc tagttgtggtttgtccaaactcatcaatgtatcttagaagttcctattccgaagttcctattctcta gaaagtataggaacttcaggcattatgacaaagccaacctatagaagaaagagttcattggctta tagcttcagtgggtgagtccataaccatcatggtggggagcttggcggcaggcaggaaagtct ggcatgggaagagcttgcctgttgatacaaccaccataaaataaagagaagactaactgggaat ggtgtgagattttgaagc.

The steps of in vitro fertilization, pronuclear injection, and embryo transplantation to the pseudopregnant mice were performed by the Transgenic, Knockout, and Tumor Model Center (TKTC) of Stanford University. Mouse pups from the injected embryos were tail clipped before weaning, and genomic DNA was extracted using the DNeasy Blood & Tissue Kit (Qiagen, 69506). To determine the result of gene editing on each mouse, the genomic DNA was screened by PCR and sequenced. A mouse containing a deletion of a 161483 bp *Loxhd1* gene fragment was identified. The Sanger sequencing results affirmed that the deletion started at the first sgRNA target site (between Exons 1and 2) and ended at the second sgRNA target site (after Exon 41). A total of 859 bps from the second ssODN sequence containing part of the mScarlet CDS up to the FRT site was inserted between the two sgRNA target sites. This allele, named $Loxhd1^{Delta}$, corresponds to the deletion of a 161483 bp in the *Loxhd1* gene (from chr18:77282757 to chr18:77444193, GRCm38/mm10), removing the protein-coding Exons 2 to 41. Germline transmission was confirmed by breeding the founder mice with the C57BL/6 J mice and backcrossing for five generations before the phenotyping analysis. $Loxhd1^{Delta}$ allele genotyping was done by PCR (See Supplementary Fig. 1) using the following primers: 5′-F: GATCTCTGCCGATCCTACAAGT; Loxhd1-Delta allele 5′-R: GGAGAAATGAGGGTATGTGTCCA; Loxhd1-Delta allele 3′-F: CGTGGA ATTCCCAAGTTCATCA; Loxhd1-Delta allele 3′-R: CCTCTCCTTCAGGG ATTGGTTTA: Delta allele (5′-F/3′-R) = 1629 bp, WT allele 5′-F/5′-R = 488 bp or 3′-F/3′-R = 856 bp.

For the $Loxhd1^{HA}$ allele, a 30 bp DNA fragment coding a glycine linker and an HA-tag (YPYDVPDYA) was inserted in Exon 1 of *Loxhd1* between the codons for the 16th amino acid, lysine, and 17th amino acid, glycine, as they show less evolutionary conservation than the rest of the protein. The chemically modified sgRNA (Gg18NGG-39, CRISPRScan, aatacgactcactataGGTCCTCCTCGTACAAGCCCgttttagag ctagaa) was ordered from Synthego (Redwood city, CA). A 127 bp asymmetric ssODN[64] containing the 30 bp tag insertion (CAGGTAGC AAAATGATGGCCCAGAAGAAGAAGCGGAGGAAGAAAGACATTGACTT CCTGGGATACCCATACGATGTTCCAGATTACGCTGGCTTGTACGAGG AGGAGCTGCTGAACTACGACTCGGA), flanked by a 36 bp homology arm on the PAM-distal side and a 61 bp homology arm on the PAM-proximal side complementary to the nontarget strand, was synthesized by IDT (Coralville, IA). A mix of EnGen Cas9 NLS (10 ng/µl, NEB, M0646T), sgRNA (10 ng/µl, Synthego), and ssODN (20 ng/µl, IDT) diluted in nuclease-free injection buffer was injected into the pronucleus of one-cell C57BL/6 J embryos. The steps of in vitro fertilization, pronuclear injection, and embryo transplantation to the pseudopregnant mice were performed by the TKTC of Stanford University. The genomic DNA of founder animals was screened by PCR and sequencing. Germline transmission was verified by breeding the founder mice with the C57BL/6 J mice, and the mice were backcrossed for at least two generations before phenotyping analysis. Genotyping was performed by PCR screening (Loxhd1-HA forward: GGTCCCAGAA-GAGGCAGGTA; Loxhd1-HA reverse: TCCAACTCATCCTCGCCATC; HA-allele: bp, WT allele). WT amplicon: 132 bp, Ex1-HA: 162 bp separated on a 2.5% agarose gel.

Both male and female subjects were used, and no differences in phenotype were found between the sexes. The genotypes and ages of mice used in specific experiments are indicated in the Figs and the main text.

Cell Lines

The HEK293T cell line from ATCC (#CRL-3216) was used for heterologous expression. The cells were cultured in DMEM + GlutaMax (Thermo Fisher, 10566016) with 10% fetal bovine serum and 1% *Penicillin/Streptomycin* added. The cells were maintained at 37 °C with 5% CO_2 and were passaged at 80% confluency.

Antibodies

Details for each antibody used in this study, including dilution and specificity validation, are provided in Supplementary Table 2.

Auditory measurements

The P21 mice were anesthetized with an intraperitoneal (IP) injection of 100-mg/kg ketamine (VetaKet CIII, AKORN, NDC 59399-114-10) and 12.5-mg/kg xylazine (AnaSed injection, AKRON, NDC 59399-110-20), and the P30 mice were anesthetized with 100-mg/kg ketamine/12.5-mg/kg xylazine/2.5-mg/kg acepromazine (VetOne, NDC 13985-587-50). The anesthetized mice were placed on a 37 °C heating pad during and after recording until they had fully recovered.

The closed field tone ABRs were tested as in ref. 45: The RZ6 Multi I/O Processor (RZ6-A-P1, TDT, Tucker-Davis Technologies, Alachua, FL), the RA4PA standard Medusa Preamplifier (TDT), a RA4LI low-impedance headstage (TDT), a needle electrode kit (ELE-N, TDT), and high-frequency speakers (MF1, TDT) were set up on the basis of the customer guide of TDT. The ABR testing system was controlled by BioSigRZ (TDT). Before each experiment, the MF1 speaker was calibrated with a 1/4″ free field microphone (PCP Piezotronics, Depew, NY). Moreover, the recording needle electrode was inserted under the skin on the vertex of the head, the reference electrode was inserted below the ipsilateral ear with a stimulating speaker, and the ground electrode was inserted below the contralateral ear. Five-millisecond tone pip stimuli were examined across a range of frequencies, including 4, 5.7, 8, 11.3, 16, 22.6, 32, and 45.3 kHz, at sound pressure levels (SPL) ranging from 0 to 80 dB in increments of 10 dB. The signals were filtered with 3-kHz low pass and 300-Hz high pass filters, along with a 60-Hz notch filter. The presentation rate was 21/sec, and 512 trails of 10-ms ABR were averaged. The ABR thresholds were defined as the lowest sound intensity at which the wave corresponding to the first evoked auditory potential could be reliably discerned. (NR: non-responsive).

Distortion products of otoacoustic emissions (DPOAEs) were tested as in ref. 45: Two high-frequency speakers (MF1, TDT) connected to the RZ6 Multi I/O Processor were used to deliver two simultaneous continuous pure tones (*F1* and *F2*), and a probe-tip microphone (type 4182, Bruel & Kjaer, Nærum, Denmark) connected to a condition amplifier (Nexus, Bruel & Kjaer) was used to detect DPOAEs from the external auditory canal. Before each experiment, MF1 speakers were calibrated with 1/4″ free field microphone (PCP

Piezotronics, Depew, NY). Two 1-s sine wave stimulus tones, each with different frequencies (F1 = 0.909 of center frequency and F2 = 1.09 of center frequency), were presented at equal intensity levels. These stimuli ranged from 0 to 80 dB SPL in 10 dB increments and were centered around frequencies of 4, 5.7, 8, 11.3, 16, 22.6, 32, and 45.3 kHz. The amplitude of the cubic distortion product was detected at *2F1-F2*. DPOAE thresholds corresponded to the sound intensity at which the amplitude of the cubic distortion product 2f1-f2 was 2 SDs above the noise floor.

Scanning electron microscopy (SEM)

SEM sample preparation and imaging were conducted as in ref. 65: The inner ears were isolated in dissection buffer (DB) (1 X HBSS with Ca^{2+} and Mg^{2+}, with osmolarity adjusted to 310 mOsm with D-glucose) and fixed in 4% PFA diluted from 32% stock in this buffer for 30 min at RT. The inner ears were then dissected to remove bone structures, the stria vascularis, and Reissner's and tectorial membranes. The samples were refixed in 2.5% glutaraldehyde and 4% PFA in DB overnight at 4 °C, washed, dehydrated in ethanol (30%, 50%, 75%, 95%, 100%, and 100%, 5 min incubations), and processed to the critical drying point using Autosamdri-815A (Tousimis). The cochleae were mounted on studs using silver paint and coated with 4-nm palladium (sputter coater EMS150TS, Electron Microscopy Sciences). The samples were imaged with a 5-kV accelerated voltage and a 13-pA beam current using a secondary electron detector on an FEI Magellan 400 XHR Field Emission Scanning Electron Microscope at the Stanford Nano Shared Facilities. The microscope is periodically calibrated for measurements using a SIRA-type calibration specimen for ultra-high-resolution modes with 2% error between 50- and 350-k magnification at our imaging settings.

Quantification of hair bundle morphology

To compare hair bundle morphology between wild-type control and the *Loxhd1*$^{Delta/Delta}$ mice, we quantified different stereocilia parameters from SEM micrographs using ImageJ2 software[66]: For IHCs, we quantified the number of stereocilia for rows 1–3, as well as their widths, which was measured at their widest position.

For OHCs, we approximated the heights of rows 2 and 3 stereocilia from OHCs that were imaged close to the orthogonal plane with respect to the hair bundle face from the 200–300th most apical OHCs (counted from low magnification SEM pictures). On the basis of 726 IHCs found along the entire adult mouse cochlea[1], we imaged the 27–41% most apical OHCs across development, which are expected to contribute to the 10.7- to 14-kHz characteristic–frequency range in adults [67]. As an approximation of the absolute stereocilia height, we measured the height of row 3 and added the rows 2 to 3 step to obtain row 2 height. The coefficient of variation of the stereocilia height was determined by dividing the standard deviation by the mean and was expressed as a percentage.

To evaluate the morphological changes of the IHC row 2 stereocilia tips between the *Loxhd1*$^{Delta/Delta}$ and wild-type mice, we traced the contours of the tip region from SEM images with Illustrator (Adobe). The same age and genotype stereocilia tip contours were aligned and stacked according to the symmetrical midlines and vertices while maintaining the scaling value.

Electrophysiology

The IHCs were recorded using a whole-cell voltage clamp as in ref. 45: All the experiments were performed at RT (19 °C–22 °C), on the apical cochlear turn, corresponding to the 6- to 10-kHz frequency range in the adult mouse.

The tissue was dissected and perfused with an extracellular solution containing the following: 145-mM NaCl, 2-mM KCl, 2-mM $CaCl_2$, 1-mM $MgCl_2$, 10-mM HEPES, 6-mM glucose, 2-mM pyruvate, 2-mM ascorbic acid, and 2-mM creatine monohydrate. The pH of the external solution was adjusted to 7.4, and the osmolarity ranged from 309 to 310 mOsm. We used borosilicate patch pipettes with a resistance of 2.5–3.5 MΩ, loaded with an internal patch solution containing the following: 116-mm CsCl, 3.5-mM $MgCl_2$, 3.5-mM ATP, 5-mM creatine phosphate, 0.1-mM tetracesium BAPTA, 10-mM HEPES, and 20-mM ascorbic acid (pH 7.2, 290 mOsm).

The MET currents were low-pass filtered at 100 kHz, measured with an Axopatch 200B patch-clamp amplifier, digitized with a daq3000 instrument (IOtech) at 500 kHz, and recorded using jClamp. For whole cell recording, the cells were held at −80 mV. The uncompensated series resistance was <10 MΩ, and cells with >100 pA of leak current were discarded. For the fluid jet stimulation of hair bundles, we used a piezoelectric disk bender delivering the fluid stimulation via a pipette with a diameter of 10–14 μm. We also used 1 kHz with an 8-pole Bessel filter (frequency devices) to filter the voltage stimulus (600–1600 mV).

Dissection and fixation of the Organ of Corti

The temporal bones were removed from the skull and put in a dish with ice-cold dissection buffer (1 × HBSS with Ca^{2+} and Mg^{2+}, with osmolarity adjusted to 310 mOsm with D-glucose) as in ref. 68: The inner ears were then dissected out and transferred to a dish with a fixative (4% PFA in dissection buffer), a hole was poked on the bony cochlear shell at the apex, and the fixative was perfused slowly through round and oval windows. The perfused inner ears were incubated in the fixative for 40 min (20 min for the TMIE-HA samples) at RT.

Whole-mount immunofluorescence staining and imaging

The whole-mount immunofluorescence staining and imaging of the mouse cochlear hair bundles in this study followed our previously published detailed protocol[68]. Briefly, the fixed inner ear samples were transferred to new dishes with 1 × PBS, and the bony cochlear shell, stria vascularis, Reissner's membrane, tectorial membrane, and the modiolus were sequentially removed. The finely dissected organs of Corti were transferred to a glass well plate with PBS containing 0.05% Triton X-100 and permeabilized for 40 min at RT. After permeabilization, the samples were blocked in PBS with 0.05% Tween 20 (PBST) containing 4% bovine serum albumin Fraction V (BSA) overnight or at least 6 hours at 4 °C. The tissues were then incubated with primary antibodies in PBST with 1% BSA (incubation buffer) overnight at 4 °C. The samples were then washed 4 times, 5–10 min per wash, in the incubation buffer at RT. Subsequently, the tissues were incubated with fluorescent dye-conjugated secondary antibodies (see below) in the incubation buffer at RT for 1–2 hours. After one wash with the incubation buffer, the samples were incubated with fluorescent dye-conjugated phalloidin (see below) in incubation buffer at RT for 25 min. The samples were then washed thrice, 5–10 min per wash, with incubation buffer. For the TMIE-HA samples, the detergent of permeabilization buffer, blocking buffer, and incubation buffer was changed to 0.05% saponin. The glass well plate was on a horizontal shaker with a 60-rpm speed during permeabilization, incubation, and washing steps. For TMC1-HA, TMC2-MYC, TMIE-HA, and LOXHD1-HA, each experiment contained at least one parallel stained cochlea sample from a similar age mouse without any tag as a background control.

After washing, each sample was mounted on a glass slide under a coverslip by using ProLong Gold Antifade Mountant (Thermo Fisher Scientific). Z-stacks were captured using the Airyscan Super-resolution mode of a Zeiss LSM880 microscope with Objective C Plan-Apochromat 63x/1.4 Oil DIC M27 lens and Zen black software (Zeiss). The image acquisition parameters were determined as the best X*Y and Z axis resolution possible for the shortest wavelength used channel.

Immunofluorescence image processing and quantification

Zeiss Zen software (blue edition, version 2.3) was used to process the Airyscan CZI format images. The processed CZI format images were

converted into an Imaris file (IMS) format by ImarisFileCoverter (Oxford Instruments version 9.8.0 or version 9.9.1), opened, and 3D reconstructed with Imaris (Oxford Instruments, version 9.8.0 or version 9.9.1 or version 10.0.0).

To identify the IHC row 2 stereocilia tip signal of target proteins, the surface tool of Imaris was used to generate the 3D rendering of each channel by utilizing the automatic algorithm without smoothing the surfaces. The "background subtraction" option was selected for thresholding with the following parameters: (1) the "diameter of the largest sphere fitting into a 3D object" was set to 265 nm; (2) for the phalloidin channel, the threshold was set at 10% of its highest intensity; (3) for HA and MYC-tagged proteins, the threshold was defined as the average intensity of the same fluorescent channel on row 2 stereocilia from the genetic negative control (no tag); (4) for LHFPL5, the threshold was defined as the average intensity of the row 1 region without puncta signals; (5) the minimal diameter defining an object or seed point was set to 200 nm; (6) the seed point was adjusted using the quality filter set at 18 for HA and MYC-tagged proteins and at 300 for LHFPL5; and (7) the other software parameters were set to default values.

From the 3D model, a given puncta was scored as present at a row 2 tip when in contact with the first 400 nm of the stereocilia tip or when placed above the stereocilia tip with a maximum gap distance of 100 nm (see Supplementary Movie and Supplementary Fig. 4a). The percentage of row 2 tip with puncta was determined and compared between genotypes.

To quantify the TMC1-HA whole hair bundle intensity of P7 OHCs, individual OHC hair bundle volumes were manually segmented from the phalloidin signal on each Z stack. The sum intensity of TMC1-HA in each OHC hair bundle volume was then determined. To combine data from different experiments, the average intensity of background control ($I_{\text{Background}}$) and the average intensity of apical *Tmc1*$^{HA/HA}$; *Loxhd1*$^{+/+}$ ($I_{\text{Wild-type}}$) were used to normalize the intensity values of each hair bundle through the following Eq. (1):

$$I_{\text{Normalized}} = 100 * \left(I - I_{\text{Background}}\right) / I_{\text{Wild-type}} \quad (1)$$

The quantification of BAIAP2l2 immunofluorescence staining was based on the signal distribution pattern relative to the height of phalloidin-labeled row 2 stereocilia. The signal was categorized as either "above or at the row 2 tip" or "below this region," with the latter being considered as a shaft signal; it was also noted when the signal was present at both locations or absent altogether. The percentage of each pattern was calculated per hair bundle.

SUB-immunogold-SEM labeling, processing, imaging, and quantification

The fixed inner ear samples were transferred to new dishes with dissection buffer to dissect the organs of Corti out. Thereafter, the samples were transferred to 2-ml tubes with TBST (150-mM NaCl, 10-mM Tris-HCl, 0.05% Tween-20, pH 7.5) containing 0.5% Triton X-100, permeabilized for 1 hour at RT. After permeabilization, the samples were washed with TBST once and then blocked in TBST containing 4% BSA for at least 6 hours or overnight at 4 °C. The samples were transferred to 0.3-ml PELCO mini vials (TED PELLA, #21441) with primary antibodies in TBST with 1% BSA overnight at 4 °C. Subsequently, the samples were transferred into 2-ml tubes, rinsed once, and washed thrice (15 min per wash) with 1% BSA TBST. The samples were then transferred to 0.3-ml PELCO mini vials with 10-nm gold conjugated goat anti-rabbit IgG (BBI: 1:200 in 1% BSA TBST) and incubated overnight at 4 °C. After 2nd antibody incubation, the samples were rinsed once and washed thrice (15 min per wash) with 1% BSA TBST in 2-ml tubes. The samples were then rinsed twice with 0.1-M sodium cacodylate buffer (pH 7.2) and fixed with 10% glutaraldehyde, 4% PFA in 0.1-M sodium cacodylate buffer for at least 24 hours at 4 °C, then washed with 0.1-M sodium cacodylate buffer, dehydrated in ethanol (30%, 50%, 75%, 95%, 100%, and 100%, 5-min incubations), and then processed to the critical drying point using Autosamdri-815A (Tousimis). The cochleae were mounted on studs using silver paint and coated with 2- to 3-nm of palladium (sputter coater EMS150TS, Electron Microscopy Sciences). The samples were imaged with a 5-kV accelerated voltage and a 100-pA beam current using a concentric backscattered electron detector on an FEI Magellan 400 XHR Field Emission SEM. The gold beads, characterized by their circular shape with an approximate diameter of 10 nm, were easily described as sources of backscattered electrons, and they were distinguishable from the signal originating from the stereocilia surface. The micrograph contrast was adjusted via Photoshop (Adobe) to display the gold better when needed. As stage tilting is impossible in backscattered electron imaging mode, hair bundle orientation could not be adjusted for optimal imaging. The distance measurements of the gold to stereocilia tips were performed with ImageJ2 after scale calibration, placing the measuring ends at the center of the gold bead and at the pointiest location of the stereocilia tip. These distances were approximations of the absolute distances as we measured the shortest distance between the gold beads and the stereocilia tip on 2D pictures without accounting for the stereocilia volume and the perspective distortion of the images. For the gold bead distribution pattern, we determined the number of stereocilia in each hair bundle with the following: at least one bead within the first 100 nm, at least one bead below 100 nm from the tip, at least one bead at any position, or without any bead. The percentage of each pattern per cell was determined, averaged and compared.

DNA constructs and plasmids

All plasmids were fully sequenced before use using the whole-plasmid sequencing service of Primordium Labs (Monrovia, CA). pCMV-hCIB2-V5[7] was gifted by Dr. Zubair Ahmed at University of Maryland, and pN3-HA-mCIB2[10] and pCMV-mPCDH15-CD2[38] were from Dr. Ulrich Müller at John Hopkins University.

pcDNA3-mLoxhd1(with CC)-MYC. was modified from pcDNA3-mLoxhd1(without CC)-MYC[45]. A coiled-coil (CC) encoding sequence containing fragment (Exons 18–21, with alternative CC Exons 19 and 20) was amplified from a P7 mouse cochlear cDNA library with PCR primer pair NG-230/NG-233. Similarly, an Exon 21–37 fragment was amplified with PCR primer pair NG-232/NG-229. Thereafter, the two fragments were hybridized and amplified by PCR with primer pair NG-230/NG-229, producing an Exon 18–37 fragment. Next, this Exon 18–37 fragment was integrated with pcDNA3-mLoxhd1(without CC)-MYC with Gibson Assembly (Gibson Assembly Master Mix (NEB, E5510S)). The Exon 18–37 fragment was amplified with PCR primer pair PW-40/PW-41 and pcDNA3-mLoxhd1(without CC)-MYC with PCR primer pair PW-42/PW-43.

NG-229, GCCAGGGTCCCACTGTCTCCATTTT
NG-230, GTCCACTACGAGATTGAGATTTGGACGG
NG-232, ACAGATACCTTCACCATCTATGCCATTGA
NG-233, GTGGTCTCGTTATTCACGTCGGTGATGT
PW-40, CCAGAAATTGGTCCACTACGAGATTGAG
PW-41, CTCCATCAATGACTGCACATATCTCACAC
PW-42, ATGTGCAGTCATTGATGGAGAGGAGATG
PW-43, CGTAGTGGACCAATTTCTGGATCTCCAC

pcDNA3-mLoxhd1(with CC)-HA. was modified from pcDNA3-mLoxhd1(with CC)-MYC by replacing the MYC-tag with the HA-tag with HA containing PCR primer pair PW-85/PW-86 amplification and following in vitro assembly with the In-Fusion Snap Assembly Master Mix (Takara, 638948).

PW-85, TACCCATACGATGTTCCAGATTACGCTTGAGAATTCCA CCACACTG

PW-86, TCTGGAACATCGTATGGGTAAACGGCCGCGACAGACG GGAAGAGCTC

pN3-FLAG-mTmc1. was modified from pN3-HA-mTmc1 (a gift from Dr. Ulrich Müller at John Hopkins University) by replacing the HA-tag with the FLAG-tag. FLAG-containing primer pair PW-139/PW-140 was used to amplify the mTmc1 CDS from pN3-HA-mTmc1. The amplified insert was digested with BglII/NotI, purified by electrophoresis, and gel extracted. The insert was ligated into BglII/NotI digested pN3 backbone with T4 ligase (NEB, M0202S).

PW-139, ACTCAGATCTCGAGATGGATTATAAAGATGATGATGA TAAAGCTCAAGCTTCGAATTCTGCAGTC

PW-140, TATGATCTAGAGTCGCGGCCGCT

pN3-FLAG-mTmc2. was modified from pN3-MYC-mTmc2[38] by replacing the MYC-tag with the FLAG-tag. FLAG-containing primer pair PW-141/PW-140 was used to amplify the CDS of mTmc2 from pN3-MYC-mTmc2. The amplicon was inserted into BglII/NotI digested pN3 backbone with the NEBuilder HiFi DNA Assembly Master Cloning Kit (NEB, E5520S).

PW-141, ACTCAGATCTCGAGATGGATTATAAAGATGATGATGATA AACAAGCTTCGAATTCTGCAGTCGA

PW-140, TATGATCTAGAGTCGCGGCCGCT

pN3-mTmie-FLAG. was modified from pN3-mTmie-HA[12] by replacing the HA-tag with the FLAG-tag by FLAG-containing PCR primer pair PW-350/PW-351 amplification followed by in vitro assembly with the In-Fusion Snap Assembly Master Mix (Takara, 638948).

PW-350, GACTACAAAGACGATGACGACAAGTGAGCGGCCGCGA CTCTAGATCATAAT

PW-351, CTTGTCGTCATCGTCTTTGTAGTCCATTTTCTCTCCTTT CTTCTTGGCCTC

pcDNA3-FLAG-mLHFPL5. was modified from pcDNA3-HA-mTMHS (mLHFPL5)[15] by replacing the HA-tag with the FLAG-tag using FLAG sequence-containing PCR primer pair PW-348/PW-349 amplification and in vitro assembly with the In-Fusion Snap Assembly Master Mix (Takara, 638948).

PW-348, GACTACAAAGACGATGACGACAAGGTGAAGTTGCTGCC AGCCCA

PW-349, CTTGTCGTCATCGTCTTTGTAGTCCATGGTGGGAATTC CAGCACAC

Co-immunoprecipitation and western blotting

Bead preparation. All the steps were performed using 2-ml low adhesion microcentrifuge tubes (USA Scientific, 1420-2600). A total of 25 µl of magnetic beads per experimental condition were transferred to a tube. The tubes were placed on a magnetic separation rack, and storage buffer was removed. For anti-HA or anti-FLAG magnetic beads, the beads were resuspended in and blocked with 4% BSA in PBS with gentle rocking at RT for 1 hour. For G-protein magnetic beads, the beads were incubated with 3 µl of anti-PCDH15 antibody diluted in 500 µl of Pierce IP Lysis Buffer (Thermo Scientific, 87787) containing protease inhibitors (Thermo Scientific, A32955) for 15 min with gentle rocking at RT. After either process, the tubes were briefly spun to remove the liquid/beads from the cap and placed on a magnetic separation rack for 1 min, and the liquid was removed. The beads were then resuspended in 25-µL Pierce IP Lysis Buffer containing protease inhibitors.

Co-Immunoprecipitation. Single or double plasmid transfections were performed on HEK293T cells 24 hours after passage using FuGENE HD Transfection Reagent (Promega, E2311). Forty-eight hours post-transfection, the cells were rinsed once with 4 °C PBS, collected in 1 ml of 4 °C PBS using a cell scraper, and then pipetted into an Eppendorf tube. The cells were also pelleted at 4 °C at 2000 g for 2 min, resuspended in 300-µL Pierce IP Lysis Buffer containing protease inhibitors, and incubated on ice for 30 min. The resuspended cells were then further disrupted by passing them through a syringe. The lysate was then spun down at 14,000 g for 20 min to pellet remaining intact cellular material. A total of 20 µL of lysate was retained for input control on the western blot, and 200-µL lysate was used for immunoprecipitation: the 200-µL lysate was diluted with 300-µL Pierce IP Lysis Buffer containing protease inhibitors, and added to appropriate beads and incubated with gentle rocking for 1 hour at 4 °C. After incubation, the tubes were spun briefly to remove the beads from the lid and then placed on a magnet rack for 1 min. The lysate was removed, and the samples were washed by resuspending through pipetting in 500-µL lysis buffer. The samples were placed on a magnetic separation rack for 1 min. This wash step was repeated thrice. On the third resuspension, the samples were removed to a new tube.

Western blot. After the final wash step of co-immunoprecipitation, the tubes were placed on a magnetic separation rack, the buffer was removed, and the samples were resuspended in 40-µL 2x Laemmli Sample Buffer (Bio-Rad, 1610737) containing 0.05% ß-Mercaptoethanol (Bio-Rad, 161-0710). A total of 20-µL 2x Laemmli sample containing 0.05% ß-Mercaptoethanol was added to the input samples, and 20-µL of each sample was run on a Mini-PROTEAN® TGX™ Precast Protein Gel, 4–20% (Bio-Rad, 4561094). For all experiments, the input lane corresponded to 10% of the lysate used in IP, all of which was loaded on the gel. The proteins were transferred to the Trans-Blot Turbo Mini 0.2 µm PVDF membrane (Bio-Rad, 1704156) using the Trans-Blot® Turbo™ Transfer System (Bio-Rad, 1704150). The blots were blocked overnight at 4 °C with gentle rotation in Intercept® (TBS) Blocking Buffer (LI-COR Biosciences, 927-60001). The blots were incubated with a blocking solution containing 0.1% Tween 20 and primary antibody (1:500 dilution) for 1 hour at RT with gentle rocking. The blots were then washed thrice five min in TBS with 0.1% Tween 20. The blots were then incubated with blocking solution containing 0.1% Tween 20 and secondary antibody (LI-COR Biosciences, 925-32211; 1:5000) for 45 min at RT with gentle rocking in the dark, and they were then washed thrice for 5 min each in TBS with 0.1% Tween 20, with a final rinse in TBS alone. The blots were then exposed using a LI-COR Odyssey CLx system (LI-COR Biosciences).

Quantification and statistical analysis

Quantifications were done from distinct samples. Statistical analyses and sample sizes for all the experiments are described in the Fig. legends and in Supplementary Table 1. Normality tests were used, and parametric or non-parametric tests were performed as appropriate. Unpaired two-tailed *t* tests or the Mann–Whitney test was performed. One-way ANOVA Tukey's multiple comparisons test was used to compare means across three genotypes. Two-way ANOVA was used to make comparisons across more than two groups followed by multiple test comparisons, either Dunnett's for comparisons to a reference mean or otherwise Šídák's. No statistical test was used to pre-determine the sample size; instead, the sample size was determined by animal availability and previous studies in the field. The statistical analysis was performed using GraphPad Prism 9.4 for Mac, GraphPad Software, San Diego, California, USA.

Reporting summary

Further information on research design is available in the Nature Portfolio Reporting Summary linked to this article.

Data availability

Uncropped blots and measurements used to generate graphs are included in supplemental figure. The data that support the findings of this study is available in a publicly accessible repository: Dryad: https://doi.org/10.5061/dryad.v15dv4256. Source data are provided with this paper.

References

1. Coste, B. et al. Piezo proteins are pore-forming subunits of mechanically activated channels. *Nature* **483**, 176–181 (2012)
2. Ranade, S. S. et al. Piezo2 is the major transducer of mechanical forces for touch sensation in mice. *Nature* **516**, 121–125 (2014).
3. Kawashima, Y. et al. Mechanotransduction in mouse inner ear hair cells requires transmembrane channel–like genes. *J. Clin. Investig.* **121**, 4796–4809 (2011).
4. Pan, B. et al. TMC1 and TMC2 are components of the mechanotransduction channel in hair cells of the mammalian inner ear. *Neuron* **79**, 504–515 (2013).
5. Jia, Y. et al. TMC1 and TMC2 Proteins Are Pore-Forming Subunits of Mechanosensitive Ion Channels. *Neuron* **105**, 310–321. (2020).
6. Pan, B. et al. TMC1 Forms the Pore of Mechanosensory Transduction Channels in Vertebrate Inner Ear Hair Cells. *Neuron* **99**, 736–753. (2018).
7. Giese, A. P. J. et al. CIB2 interacts with TMC1 and TMC2 and is essential for mechanotransduction in auditory hair cells. *Nat. Commun.* **8**, 1–12 (2017).
8. Beurg, M., Barlow, A., Furness, D. N. & Fettiplace, R. A Tmc1 mutation reduces calcium permeability and expression of mechanoelectrical transduction channels in cochlear hair cells. *Proc. Natl Acad. Sci. USA* **116**, 20743–20749 (2019).
9. Michel, V. et al. CIB2, defective in isolated deafness, is key for auditory hair cell mechanotransduction and survival. *EMBO Mol. Med* **9**, 1711–1731 (2017).
10. Liang, X. et al. CIB2 and CIB3 are auxiliary subunits of the mechanotransduction channel of hair cells. *Neuron* **109**, 2131–2149.e15 (2021).
11. Wang, Y. et al. Loss of CIB2 Causes Profound Hearing Loss and Abolishes Mechanoelectrical Transduction in Mice. *Front Mol. Neurosci.* **10**, 1–14 (2017).
12. Zhao, B. et al. TMIE is an essential component of the mechanotransduction machinery of cochlear hair cells. *Neuron* **84**, 954–967 (2014).
13. Cunningham, C. L. et al. TMIE Defines Pore and Gating Properties of the Mechanotransduction Channel of Mammalian Cochlear Hair Cells. *Neuron* **107**, 126–143 (2020).
14. Qiu, X., Liang, X., Llongueras, J. P., Cunningham, C. & Müller, U. The tetraspan LHFPL5 is critical to establish maximal force sensitivity of the mechanotransduction channel of cochlear hair cells. *Cell Rep.* **42**, 112245 (2023).
15. Xiong, W. et al. TMHS is an integral component of the mechanotransduction machinery of cochlear hair cells. *Cell*. **151**, 1283–1295 (2012).
16. Kim, K. X. & Fettiplace, R. Developmental changes in the cochlear hair cell mechanotransducer channel and their regulation by transmembrane channel–like proteins. *J. Gen. Physiol.* **141**, 141–148 (2013).
17. Kim, K. X. et al. The role of transmembrane channel-like proteins in the operation of hair cell mechanotransducer channels. *J. Gen. Physiol.* **142**, 493–505 (2013).
18. Fettiplace, R., Furness, D. N. & Beurg, M. The conductance and organization of the TMC1-containing mechanotransducer channel complex in auditory hair cells. *Proc. Natl Acad. Sci. USA* **119**, 1–10 (2022).
19. Beurg, M., Schwalbach, E. T. & Fettiplace, R. LHFPL5 is a key element in force transmission from the tip link to the hair cell mechanotransducer channel. *Proc. Natl Acad. Sci. USA* **121**, e2318270121 (2024).
20. Tilney, L. G. & Saunders, J. C. Actin filaments, stereocilia, and hair cells of the bird cochlea I. Length, number, width, and distribution of stereocilia of each hair cell are related to the position of the hair cell on the cochlea. *J. Cell Biol.* **96**, 807–821 (1983).
21. Tilney, L. G., Tilney, M. S. & Cotanche, D. A. Actin filaments, stereocilia, and hair cells of the bird cochlea. V. How the staircase pattern of stereociliary lengths is generated. *J. Cell Biol.* **106**, 355–365 (1988).
22. Pickles, J. O., Comis, S. D. & Osborne, M. P. Cross-links between stereocilia in the guinea pig organ of Corti, and their possible relation to sensory transduction. *Hear Res.* **15**, 103–112 (1984).
23. Osborne, M. P., Comis, S. D. & Pickles, J. O. Morphology and cross-linkage of stereocilia in the guinea-pig labyrinth examined without the use of osmium as a fixative. *Cell Tissue Res.* **237**, 43–48 (1984).
24. Ahmed, Z. M. et al. The Tip-Link Antigen, a Protein Associated with the Transduction Complex of Sensory Hair Cells, Is Protocadherin-15. *J. Neurosci.* **26**, 7022–7034 (2006).
25. Siemens, J., Lillo, C. & Müller, U. & 7. Cadherin 23 is a component of the tip link in hair-cell stereocilia. *Nature* **428**, 950–955 (2004).
26. Sollner, C. et al. Mutations in cadherin 23 affect tip links in zebrafish sensory hair cells. *Nature* **428**, 955–959 (2004).
27. Kazmierczak, P. et al. Cadherin 23 and protocadherin 15 interact to form tip-link filaments in sensory hair cells. *Nature* **449**, 87–91 (2007).
28. Beurg, M., Fettiplace, R., Nam, J.-H. & Ricci, A. J. Localization of inner hair cell mechanotransducer channels using high-speed calcium imaging. *Nat. Neurosci.* **12**, 553–558 (2009).
29. Assad, J. A., Shepherd, G. M. G. & Corey, D. P. Tip-link integrity and mechanical transduction in vertebrate hair cells. *Neuron* **7**, 985–994 (1991).
30. Kurima, K. et al. TMC1 and TMC2 Localize at the Site of Mechanotransduction in Mammalian Inner Ear Hair Cell Stereocilia. *Cell Rep.* **12**, 1606–1617 (2015).
31. Waguespack, J., Salles, F. T., Kachar, B. & Ricci, A. J. Stepwise morphological and functional maturation of mechanotransduction in rat outer hair cells. *J. Neurosci.* **27**, 13890–13902 (2007).
32. Pacentine, I. V. & Nicolson, T. Subunits of the mechano-electrical transduction channel, Tmc1/2b, require Tmie to localize in zebrafish sensory hair cells. *PLoS Genet* **15**, 1–34 (2019).
33. Yu, X. et al. Deafness mutation D572N of TMC1 destabilizes TMC1 expression by disrupting LHFPL5 binding. *Proc. Natl Acad. Sci. USA* **117**, 29894–29903 (2020).
34. Maeda, R. et al. Tip-link protein protocadherin 15 interacts with transmembrane channel-like proteins TMC1 and TMC2. *Proc. Natl Acad. Sci. USA* **111**, 12907–12912 (2014).
35. Mahendrasingam, S., Fettiplace, R., Alagramam, K. N., Cross, E. & Furness, D. N. Spatiotemporal changes in the distribution of LHFPL5 in mice cochlear hair bundles during development and in the absence of PCDH15. *PLoS One* **12**, 1–22 (2017).
36. Ge, J. et al. Structure of mouse protocadherin 15 of the stereocilia tip link in complex with LHFPL5. *Elife* **7**, 1–24 (2018).
37. Riazuddin, S. et al. Alterations of the CIB2 calcium- and integrin-binding protein cause Usher syndrome type 1 J and nonsyndromic deafness DFNB48. *Nat. Genet* **44**, 1265–1271 (2012).
38. Beurg, M., Xiong, W., Zhao, B., Müller, U. & Fettiplace, R. Subunit determination of the conductance of hair-cell mechanotransducer channels. *Proc. Natl Acad. Sci.* **112**, 1589–1594 (2015).
39. Li, X. et al. Localization of TMC1 and LHFPL5 in auditory hair cells in neonatal and adult mice. *FASEB J.* **33**, 6838–6851 (2019).
40. Grillet, N. et al. Mutations in LOXHD1, an Evolutionarily Conserved Stereociliary Protein, Disrupt Hair Cell Function in Mice and Cause Progressive Hearing Loss in Humans. *Am. J. Hum. Genet* **85**, 328–337 (2009).
41. Hytönen, M. K. et al. Missense variant in LOXHD1 is associated with canine nonsyndromic hearing loss. *Hum. Genet.* **140**, 1611–1618 (2021).

42. Edvardson, S. et al. A deleterious mutation in the LOXHD1 gene causes autosomal recessive hearing loss in Ashkenazi Jews. *Am. J. Med. Genet. A* **155**, 1170–1172 (2011).
43. Kim, B. J. et al. Rising of LOXHD1 as a signature causative gene of down-sloping hearing loss in people in their teens and 20 s. *J. Med. Genet*. **59**, 470–480 (2022).
44. Mori, K. et al. Mutations in LOXHD1 Gene Cause Various Types and Severities of Hearing Loss. *Ann. Otol., Rhinol. Laryngol.* **124**, 135S–141S (2015).
45. Trouillet, A. et al. Loxhd1 Mutations Cause Mechanotransduction Defects in Cochlear Hair Cells. *J. Neurosci.* **41**, 3331–3343 (2021).
46. Goodyear, R. J. et al. Asymmetric distribution of cadherin 23 and protocadherin 15 in the kinocilial links of avian sensory hair cells. *J. Comp. Neurol.* **518**, 4288–4297 (2010).
47. Indzhykulian, A. A. et al. Molecular remodeling of tip links underlies mechanosensory regeneration in auditory hair cells. *PLoS Biol.* **11**, e1001583 (2013).
48. Wu, X. et al. PKHD1L1 is a coat protein of hair-cell stereocilia and is required for normal hearing. *Nat. Commun.* **10**, 3801 (2019).
49. Verpy, E. et al. Stereocilin connects outer hair cell stereocilia to one another and to the tectorial membrane. *J. Comp. Neurol.* **519**, 194–210 (2011).
50. Miller, K. K., Wang, P. & Grillet, N. SUB-immunogold-SEM reveals nanoscale distribution of submembranous epitopes. *Nat. Commun.* https://doi.org/10.1038/s41467-024-51849-x (2024).
51. Asai, Y. et al. Transgenic Tmc2 expression preserves inner ear hair cells and vestibular function in mice lacking Tmc1. *Sci. Rep.* **8**, 12124 (2018).
52. Halford, J., Bateschell, M. & Barr-Gillespie, P. G. Ca^{2+} entry through mechanotransduction channels localizes BAIAP2L2 to stereocilia tips. *Mol. Biol. Cell* **33**, br6 (2022).
53. Carlton, A. J. et al. Loss of Baiap2l2 destabilizes the transducing stereocilia of cochlear hair cells and leads to deafness. *J. Physiol.* **4**, 1173–1198 (2020).
54. Yan, K. et al. BAIAP2L2 is required for the maintenance of mechanotransducing stereocilia of cochlear hair cells. *J. Cell Physiol.* **237**, 774–788 (2022).
55. Webb, S. W. et al. Regulation of PCDH15 function in mechanosensory hair cells by alternative splicing of the cytoplasmic domain. *Development* **138**, 1607–1617 (2011).
56. Pepermans, E. et al. The CD2 isoform of protocadherin-15 is an essential component of the tip-link complex in mature auditory hair cells. *EMBO Mol. Med.* **6**, 984–992 (2014).
57. Mahendrasingam, S. & Furness, D. N. Ultrastructural localization of the likely mechanoelectrical transduction channel protein, transmembrane-like channel 1 (TMC1) during development of cochlear hair cells. *Sci. Rep.* **9**, 1274 (2019).
58. Miller, K. K., Atkinson, P., Mendoza, K. R., Maoiléidigh, D. Ó. & Grillet, N. Dimensions of a Living Cochlear Hair Bundle. *Front Cell Dev. Biol.* **9**, 3097 (2021).
59. Zheng, W. & Holt, J. R. The Mechanosensory Transduction Machinery in Inner Ear Hair Cells. *Annu Rev Biophys.* **50**, 31–51 (2021).
60. Powers, R. J. et al. Stereocilia membrane deformation: implications for the gating spring and mechanotransduction channel. *Biophys. J.* **102**, 201–210 (2012).
61. Gillespie, P. G. & Müller, U. Mechanotransduction by hair cells: models, molecules, and mechanisms. *Cell* **139**, 33–44 (2009).
62. Cho, K. I. et al. The circling mouse (C57BL/6J-cir) has a 40-kilobase genomic deletion that includes the transmembrane inner ear (tmie) gene. *Comp. Med.* **56**, 476–481 (2006).
63. Grillet, N. et al. Generation and characterization of Rgs4 mutant mice. *Mol. Cell Biol.* **25**, 4221–4228 (2005).
64. Richardson, C. D., Ray, G. J., DeWitt, M. A., Curie, G. L. & Corn, J. E. Enhancing homology-directed genome editing by catalytically active and inactive CRISPR-Cas9 using asymmetric donor DNA. *Nat. Biotechnol.* **34**, 339–344 (2016).
65. Grillet, N. High-resolution imaging of the mouse-hair- cell hair bundle by scanning electron microscopy bundle by scanning electron microscopy. *STAR Protoc.* **3**, 101213 (2022).
66. Rueden, C. T. et al. ImageJ2: ImageJ for the next generation of scientific image data. *BMC Bioinform.* **18**, 529 (2017).
67. Müller, M., Von Hünerbein, K., Hoidis, S. & Smolders, J. W. T. A physiological place-frequency map of the cochlea in the CBA/J mouse. *Hear Res.* **202**, 63–73 (2005).
68. Miller, K. K., Wang, P. & Grillet, N. High-resolution immunofluorescence imaging of mouse cochlear hair bundles. *STAR Protoc.* **3**, 101431 (2022).

Acknowledgements

The work was funded by the National Institute on Deafness, and Other Communication Disorders Grants 1R21DC019457-01 (N.G.), 1R01DC016409-01A1 (N.G.), 1R01DC021835-01 (CLC), R21DC019195, the National Institute on Aging Grant 1R01AG081608-01 (N.G.), the Stanford Maternal and Child Health Research Institute (NG), and the OHNS departmental support (N.G.). Part of this work was performed at the Stanford Nano Shared Facilities (SNSF), supported by the National Science Foundation under award ECCS-2026822. We would like to thank Dr. Hong Zeng and the Stanford Transgenic, Knockout & Tumor Model Center, and Dr. Patrick Atkinson and the Otolaryngology Department Imaging and Audiometry core facilities. We would also like to thank Dr. Ulrich Müller, Dr. Zubair Ahmed, and Dr. Arnaud Giese for providing constructs, Dr. Robert Fettiplace and Dr. Marlyn Beurg for sharing the *Tmc1*^{KO} mice, Dr. Anthony Ricci for training E.H. with electrophysiology, and providing feedback on the manuscript along with Dr. Dáibhid Ó Maoiléidigh, and Dr. Bertrand Coste. N.G. thanks Lais Priolli for constant support. Finally, we thank Shari and Kenneth Eberts, the Oberndorf family, and the SICHL contributors for their support.

Author contributions

P.W. carried out the mouse mutant generation, cloning, immunolocalization studies, and quantifications. K.M. performed the biochemical experiments. E.H. performed the hair cell electrophysiology. S.D. conducted the auditory tests and cloning. C.L.C. provided the *Tmc1*^{HA}, *Tmc2*^{MYC,} and *Tmie*^{HA} mice. N.G. performed the SEM imaging. P.W., K.M., and N.G. designed the study. All the authors contributed to the data analysis. N.G. wrote the manuscript with help from P.W., K.M. and C.L.C.

Competing interests

The authors declare no competing interests.

Additional information

Supplementary information The online version contains supplementary material available at https://doi.org/10.1038/s41467-024-51850-4.

Correspondence and requests for materials should be addressed to Nicolas Grillet.

Peer review information *Nature Communications* thanks the anonymous reviewer(s) for their contribution to the peer review of this work. A peer review file is available.